Multibody Syst Dyn (2008) 19: 45–72
DOI 10.1007/s11044-007-9056-4

The discrete null space method for the energy-consistent integration of constrained mechanical systems. Part III: Flexible multibody dynamics

Sigrid Leyendecker · Peter Betsch · Paul Steinmann

Received: 27 September 2006 / Accepted: 16 April 2007 /
Published online: 6 June 2007
© Springer Science+Business Media B.V. 2007

Abstract In the present work, the unified framework for the computational treatment of rigid bodies and nonlinear beams developed by Betsch and Steinmann (Multibody Syst. Dyn. **8**, 367–391, 2002) is extended to the realm of nonlinear shells. In particular, a specific constrained formulation of shells is proposed which leads to the semi-discrete equations of motion characterized by a set of differential-algebraic equations (DAEs). The DAEs provide a uniform description for rigid bodies, semi-discrete beams and shells and, consequently, flexible multibody systems. The constraints may be divided into two classes: (i) internal constraints which are intimately connected with the assumption of rigidity of the bodies, and (ii) external constraints related to the presence of joints in a multibody framework. The present approach thus circumvents the use of rotational variables throughout the whole time discretization, facilitating the design of energy–momentum methods for flexible multibody dynamics. After the discretization has been completed a size-reduction of the discrete system is performed by eliminating the constraint forces. Numerical examples dealing with a spatial slider-crank mechanism and with intersecting shells illustrate the performance of the proposed method.

Keywords Conserving time integration · Constrained mechanical systems · Flexible multibody dynamics · Nonlinear structural dynamics · Differential-algebraic equations

1 Introduction

In Ref. [7] the discrete null space method developed by Betsch [6] has been applied to multibody systems comprising rigid bodies. In the present work, the procedure is extended for

S. Leyendecker (✉) · P. Steinmann
Chair of Applied Mechanics, Department of Mechanical Engineering, University of Kaiserslautern, Kaiserslautern, Germany
e-mail: slauer@rhrk.uni-kl.de

P. Betsch
Chair of Computational Mechanics, Department of Mechanical Engineering, University of Siegen, Siegen, Germany

nonlinear structural mechanics, in particular for geometrically exact beams and shells forming flexible multibody systems. The precursor works [6, 7] will be subsequently referred to as Part I and Part II, respectively.

In recent years the extension of finite element methods for nonlinear structural dynamics to the realm of flexible multibody dynamics has attracted a lot of research. This has been facilitated by previous developments of computational methods for nonlinear structural mechanics which have reached a certain state of maturity. In this connection, main ingredients of contemporary methods for structural dynamics are (i) the use of nonlinear strain measures which may account for both finite strains and arbitrarily large rigid body motions, and (ii) so-called mechanical integrators (e.g., energy–momentum or energy-decaying schemes) which make possible the stable time integration of the 'stiff' nonlinear ODEs resulting from the space discretization.

In a flexible multibody framework the components may consist of flexible bodies (e.g., beams, shells or continua) and rigid bodies. These components are typically interconnected by various types of joints (e.g., spherical, revolute, prismatic, ...). The joints impose constraints on the multibody system, thus restricting the relative motion of the components. The presence of the constraints constitutes the major challenge for the development of finite-element-based computational methods.

In essence, three alternative methods have been applied previously to deal with the constraints within a nonlinear finite element framework: (i) The constraints may be enforced by means of Lagrange multipliers. This approach has been used, for example, by Géradin and Cardona [17], Ibrahimbegović et al. [25], Puso [33], Taylor [40], Bottasso et al. [12] and Bauchau et al. [3]. (ii) Alternatively, the constraints may be accounted for by kinematic relationships within the master-slave approach developed by Jelenić and Crisfield [27], see also Ibrahimbegović et al. [25], Göttlicher [21] and Muñoz et al. [32]. (iii) The constraints may be imposed by means of the penalty method. This approach has been applied, for example, by Goicolea and Orden [18].

In all of the above cited works rotational parameters are used as an integral part of the description of both structural components and rigid bodies. Similarly, previous works on the dynamics of nonlinear shells make use of rotational parameters, at least within the time discretization. See, for example, Simo et al. [38], Simo and Tarnow [39], Kuhl and Ramm [28], Sansour et al. [36], Romero and Armero [34] and Brank et al. [13].

In the present work we present a specific discretization (in space and time) of geometrically nonlinear beams and shells that does not rely on the use of rotational parameters. Instead of using rotations for the parametrization of the underlying nonlinear configuration manifold we use redundant coordinates and directly impose algebraic constraints associated with the configuration manifold at hand using the Lagrange multiplier method. These constraints are termed internal constraints. Further constraints due to Dirichlet-type boundary conditions and due to joints in a multibody framework are termed external constraints. This approach has already been successfully applied to nonlinear beams and rigid bodies, see Betsch and Steinmann [8, 10]. It leads to differential-algebraic equations (DAEs) of motion with constant mass matrix. In [29, 30] Leyendecker et al. compared different approaches concerning the constraint enforcement (in particular the Lagrange multiplier method, the penalty method and the augmented Lagrange method) theoretically and with the help of examples of mass point system, rigid body and nonlinear beam dynamics. It turned out that only the Lagrange multiplier method yields an acceptable combination of accuracy in the constraint fulfillment and computational costs. As a consequence of the advocated DAE-formulation of rigid bodies, beams and shells, the appearing constraints are at most quadratic, which facilitates the energy–momentum conserving time-integration. However,

the resulting time-stepping scheme has a relatively large dimension (it has to be solved for redundant coordinates plus Lagrange multipliers) and it may suffer from conditioning problems (cf. Part I). Both drawbacks are eliminated by the application of the discrete null space method. Its main ingredients are a discrete null space matrix and a reparametrization of the discrete configuration variable in independent incremental unknowns with which a size reduction of the time-stepping scheme can be achieved and potential conditioning problems can be removed. Accordingly, the main goal of this work is the design of viable null space matrices with their discrete counterparts for the internal constraints in geometrically exact beams and shells. Together with the null space matrices developed for the external constraints due to joint connections in Part II, the total null space matrix for a flexible multibody system can be composed multiplicatively.

The energy-consistent temporal discretization of the DAEs governing the dynamics of constrained finite-dimensional mechanical systems is sketched in Sect. 2. Furthermore, the reduction of the resulting time-stepping scheme by the discrete null space method is outlined. Section 3 deals with the dynamics of geometrically exact beams which can be viewed as a generalization of rigid bodies to the spatially distributed case. In this connection, the rigid body formulation explained in Part II is recalled in brief. Section 4 is devoted to the formulation of geometrically exact shells as constrained mechanical systems. In particular, the discrete null space matrices pertaining to the internal constraints in beam and shell dynamics are deduced in these sections. A general procedure for the treatment of multibody systems consisting of rigid and flexible components by the discrete null space method is described in detail in Sect. 5. The following numerical examples deal with the dynamics of a spatial slider-crank mechanism consisting of beams and rigid bodies and with a multibody system comprised by intersecting shells and rigid bodies respectively.

2 Outline of the discrete null space method

An outline of the treatment of constrained dynamical systems by null space methods is given in this section. First the d'Alembert-type formulation of a finite dimensional constrained mechanical system is deduced in the temporal continuous setting. Then, according to the discrete null space method, similar steps are performed in the temporal discrete setting to deduce a reduced energy-consistent time-stepping scheme.

2.1 Constrained dynamical systems

Consider an n-dimensional mechanical system with the time-dependent configuration vector $\boldsymbol{q}(t) \in \mathbb{R}^n$ and velocity vector $\dot{\boldsymbol{q}}(t) \in \mathbb{R}^n$, where $t \in [t_0, t_1] \subset \mathbb{R}$ denotes the time. Let the system be constrained by the function $\boldsymbol{\Phi}(\boldsymbol{q}) = \boldsymbol{0} \in \mathbb{R}^m$. The constrained formulation of the equations of motion is based on the Lagrangian $L : \mathbb{R}^n \times \mathbb{R}^n \times \mathbb{R}^m \to \mathbb{R}$

$$L(\boldsymbol{q}, \dot{\boldsymbol{q}}, \boldsymbol{\lambda}) = \frac{1}{2}\, \dot{\boldsymbol{q}} \cdot \boldsymbol{M} \cdot \dot{\boldsymbol{q}} - V(\boldsymbol{q}) - \boldsymbol{\Phi}^T(\boldsymbol{q}) \cdot \boldsymbol{\lambda} \tag{1}$$

which comprises the kinetic energy including the consistent mass matrix $\boldsymbol{M} \in \mathbb{R}^{n \times n}$, a potential function $V : \mathbb{R}^n \to \mathbb{R}$ and the scalar product of the constraint function with a Lagrange multiplier $\boldsymbol{\lambda} \in \mathbb{R}^m$. For simplicity, a conservative system is assumed with a potential energy function, from which a nodal force vector can be computed. For deformable mechanical systems, the potential energy function may be split into an internal part V_{int} corresponding to hyperelastic material behavior and an external part V_{ext} accounting for external loading

such that $V = V_{\text{int}} + V_{\text{ext}}$. Note that a characteristic feature of the constrained formulation of rigid body, beam and shell dynamics advocated in Sects. 3 and 4 is that $\boldsymbol{M}$ is constant. Hamilton's principle of least action leads to the Lagrange equations of motion of the first kind:

$$\begin{aligned} &\boldsymbol{M} \cdot \ddot{\boldsymbol{q}} + \nabla V(\boldsymbol{q}) + \boldsymbol{G}^T(\boldsymbol{q}) \cdot \boldsymbol{\lambda} = \boldsymbol{0}, \\ &\boldsymbol{\Phi}(\boldsymbol{q}) = \boldsymbol{0} \end{aligned} \tag{2}$$

where $\boldsymbol{G}(\boldsymbol{q}) = D\boldsymbol{\Phi}(\boldsymbol{q})$ is the Jacobian of the constraints. The vector $\boldsymbol{G}^T(\boldsymbol{q}) \cdot \boldsymbol{\lambda}$ represents the constraint forces that prevent the system from deviations of the constraint manifold:

$$Q = \left\{ \boldsymbol{q}(t) \in \mathbb{R}^n \mid \boldsymbol{\Phi}(\boldsymbol{q}) = \boldsymbol{0} \right\}. \tag{3}$$

It is assumed that the m constraints are independent, i.e., $\operatorname{rank}(\boldsymbol{G}(\boldsymbol{q})) = m$ for all $\boldsymbol{q} \in Q$ and Q is an $(n-m)$-dimensional submanifold of the configuration space. Due to the consistency condition, which requires that the constraints are fulfilled for all times, admissible velocities are restricted to the null space of the constraint Jacobian. Together with the configuration constraints the consistency condition defines the $2(n-m)$-dimensional submanifold

$$TQ = \left\{ (\boldsymbol{q}, \dot{\boldsymbol{q}}) \in \mathbb{R}^n \times \mathbb{R}^n \mid \boldsymbol{\Phi}(\boldsymbol{q}) = \boldsymbol{0}, \boldsymbol{G}(\boldsymbol{q}) \cdot \dot{\boldsymbol{q}} = \boldsymbol{0} \right\} \tag{4}$$

of the state space.

Continuous null space matrix For every $\boldsymbol{q} \in Q$, the basis vectors of $T_{\boldsymbol{q}}Q$ form an $n \times (n-m)$ matrix $\boldsymbol{P}(\boldsymbol{q})$ with corresponding linear map $\boldsymbol{P}(\boldsymbol{q}) : \mathbb{R}^{n-m} \to T_{\boldsymbol{q}}Q$. This matrix is called null space matrix, since

$$\operatorname{range}\big(\boldsymbol{P}(\boldsymbol{q})\big) = \operatorname{null}\big(\boldsymbol{G}(\boldsymbol{q})\big) = T_{\boldsymbol{q}}Q. \tag{5}$$

Hence admissible velocities can be expressed as

$$\dot{\boldsymbol{q}}(t) = \boldsymbol{P}(\boldsymbol{q}) \cdot \boldsymbol{v}(t) \tag{6}$$

with the independent generalized (quasi-) velocities $\boldsymbol{v} \in \mathbb{R}^{n-m}$. Thus a premultiplication of the differential equation $(2)_1$ by $\boldsymbol{P}^T(\boldsymbol{q})$ eliminates the constraint forces including the Lagrange multipliers from the system. The resulting d'Alembert-type equations of motion read

$$\begin{aligned} &\boldsymbol{P}^T(\boldsymbol{q}) \cdot [\boldsymbol{M} \cdot \ddot{\boldsymbol{q}} + \nabla V(\boldsymbol{q})] = \boldsymbol{0}, \\ &\boldsymbol{\Phi}(\boldsymbol{q}) = \boldsymbol{0}. \end{aligned} \tag{7}$$

Remark 2.1 (Continuous null space matrix) Note that the null space matrix is not unique, a necessary and sufficient condition on $\boldsymbol{P}(\boldsymbol{q})$ is (5). The null space matrix can be found in different ways, either by velocity analysis (i.e., corresponding to (6), the map mapping the independent generalized velocities to the redundant velocities represents a viable null space matrix) or by performing an explicit QR-decomposition of the transposed continuous constraint Jacobian in terms of the configuration variable

$$\boldsymbol{G}^T = \boldsymbol{Q} \cdot \boldsymbol{R} = [\boldsymbol{Q}_1, \boldsymbol{Q}_2] \cdot \begin{bmatrix} \boldsymbol{R}_1 \\ \boldsymbol{0}_{(n-m)\times m} \end{bmatrix} \tag{8}$$

with the nonsingular upper triangular matrix $\boldsymbol{R}_1 \in \mathbb{R}^{m\times m}$ and the orthogonal matrix $\boldsymbol{Q} \in O(n)$, which can be partitioned into the orthogonal matrices $\boldsymbol{Q}_1 \in \mathbb{R}^{n\times m}$ and $\boldsymbol{Q}_2 \in \mathbb{R}^{n\times(n-m)}$. Then $\boldsymbol{P}(\boldsymbol{q}) = \boldsymbol{Q}_2(\boldsymbol{q})$ serves as null space matrix, which is sometimes called 'natural orthogonal complement' (see [1]). The third way to obtain a continuous null space matrix as the Jacobian of the reparametrization of the constraint manifold is often possible, but the resulting continuous null space matrix can in general not be used to infer a discrete null space matrix. This is due to the fact that the respective discrete values of the generalized coordinates are not available in the present approach.

Reparametrization of unknowns For many applications it is possible to find a reparametrization of the constraint manifold $\boldsymbol{F} : U \subseteq \mathbb{R}^{n-m} \to Q$ in terms of independent generalized coordinates $\boldsymbol{u} \in U$. Then the Jacobian $D\boldsymbol{F}(\boldsymbol{u})$ of the coordinate transformation plays the role of a null space matrix. Since the constraints are fulfilled automatically by the reparametrized configuration variable $\boldsymbol{q} = \boldsymbol{F}(\boldsymbol{u})$, the system is reduced to $n - m$ second order differential equations. This is the minimal possible dimension for the present mechanical system which consists of precisely $n - m$ degrees of freedom.

2.2 Discrete null space method

A drawback for the time-discretization of the d'Alembert-type equations of motion (7) is that the null space matrix is configuration-dependent. The discrete null space method circumvents this shortcoming. It relies on the temporal discretization of the comparatively simple structured constrained formulation (2) and the size reduction is performed in the discrete setting by the introduction of a discrete null space matrix in analogy to the procedure in the continuous case.

The DAEs (2) are discretized in time using the concept of discrete derivatives by Gonzalez [20]. Alternatively, the constrained scheme applied herein can be derived from the Galerkin-based mG(1) method as proposed by Betsch and Steinmann [9]. Using the given quantities $(\boldsymbol{q}_n, \boldsymbol{v}_n) \in Q \times \mathbb{R}^n$ which approximate $\boldsymbol{q}(t_n), \dot{\boldsymbol{q}}(t_n)$ respectively, the following constrained scheme determines $\boldsymbol{q}_{n+1}, \boldsymbol{v}_{n+1}, \boldsymbol{\lambda}$

$$\begin{aligned}
&\boldsymbol{q}_{n+1} - \boldsymbol{q}_n - \Delta t\, \boldsymbol{v}_{n+\frac{1}{2}} = \boldsymbol{0},\\
&\boldsymbol{M} \cdot (\boldsymbol{v}_{n+1} - \boldsymbol{v}_n) + \Delta t \mathsf{D}V(\boldsymbol{q}_n, \boldsymbol{q}_{n+1}) + \Delta t \mathbf{G}^T(\boldsymbol{q}_n, \boldsymbol{q}_{n+1}) \cdot \boldsymbol{\lambda} = \boldsymbol{0},\\
&\boldsymbol{\Phi}(\boldsymbol{q}_{n+1}) = 0.
\end{aligned} \tag{9}$$

Here $(\bullet)_{n+\frac{1}{2}} = ((\bullet)_n + (\bullet)_{n+1})/2$ denotes the midpoint value of the approximations to a time dependent function at the time nodes and Δt denoted the time-step. The operator D denotes the discrete derivative and $\mathbf{G}(\boldsymbol{q}_n, \boldsymbol{q}_{n+1}) = \mathsf{D}\boldsymbol{\Phi}(\boldsymbol{q}_n, \boldsymbol{q}_{n+1})$. The above scheme enjoys a number of desirable properties such as second-order accuracy in the coordinates and velocities and satisfaction of the configuration constraints at the time nodes. Furthermore, by definition of the discrete derivative (see [19]), the resulting scheme (9) conserves the total energy and (at most quadratic) momentum maps, related to symmetries of the underlying continuous system, along its solution. Further details of the constrained scheme can be found in Part I of this work. It is worth mentioning, that the constraints on velocity level emanating from the temporal differentiation of $(2)_2$ can easily be incorporated into the present time-stepping scheme, see [9]. However, according to experience, their incorporation does not alter the numerical results significantly enough to warrant the corresponding increase in numerical costs.

Discrete null space matrix The transition to the discrete d'Alembert-type scheme implicating a size reduction of the constrained scheme (9) can be accomplished in complete analogy to the continuous case. A discrete null space matrix $\mathbf{P}(\boldsymbol{q}_n, \boldsymbol{q}_{n+1}) : \mathbb{R}^{n-m} \to \mathbb{R}^n$ whose columns form a basis for the null space of the discrete derivative of the constraints, i.e.

$$\operatorname{range}\big(\mathbf{P}(\boldsymbol{q}_n, \boldsymbol{q}_{n+1})\big) = \operatorname{null}\big(\mathbf{G}(\boldsymbol{q}_n, \boldsymbol{q}_{n+1})\big) \tag{10}$$

must be found. Premultiplying $(9)_2$ by the transposed of this matrix cancels the constraint forces and thus eliminates the Lagrange multipliers from the scheme. The resulting d'Alembert-type time-stepping scheme

$$\begin{aligned} &\boldsymbol{q}_{n+1} - \boldsymbol{q}_n - \Delta t \boldsymbol{v}_{n+\frac{1}{2}} = \mathbf{0}, \\ &\mathbf{P}^T(\boldsymbol{q}_n, \boldsymbol{q}_{n+1}) \cdot \big[\boldsymbol{M}(\boldsymbol{v}_{n+1} - \boldsymbol{v}_n) + \Delta t \mathsf{D}V(\boldsymbol{q}_n, \boldsymbol{q}_{n+1})\big] = \mathbf{0}, \\ &\boldsymbol{\Phi}(\boldsymbol{q}_{n+1}) = \mathbf{0} \end{aligned} \tag{11}$$

is equivalent to the constrained scheme and can be used to determine $\boldsymbol{q}_{n+1} \in \mathbb{R}^n$ (see Sect. 3.2. in Part I).

One major goal of this work is to find appropriate explicit representations of the discrete null space matrix $\mathbf{P}(\boldsymbol{q}_n, \boldsymbol{q}_{n+1}) \in \mathbb{R}^{n\times(n-m)}$ for multibody systems comprised of rigid bodies, geometrically exact beams and shells.

Remark 2.2 (Discrete null space matrix) The fulfillment of condition (10) and the consistency property of the discrete derivative imply that a viable discrete null space matrix coincides with its continuous counterpart for decreasing time-steps, i.e. $\mathbf{P}(\boldsymbol{q}_n, \boldsymbol{q}_{n+1}) \to \boldsymbol{P}(\boldsymbol{q}_n)$ as $\boldsymbol{q}_{n+1} \to \boldsymbol{q}_n$. In general, an explicit representation of the discrete null space matrix is desirable for practical applications since it minimizes the computational costs. Indeed, such an explicit representation is feasible for many application. For example, for rigid bodies, kinematic pairs and open kinematic chains, the discrete null space matrices pertaining to the specific constraints are given in Part II. For these examples, the discrete null space matrices rely on the midpoint evaluation of the continuous null space matrix or a slight modification of that. If no explicit discrete null space matrix can be found, nevertheless an implicit representation can be used in any case. It is based on the QR-decomposition of the transposed constraint Jacobian at $\boldsymbol{q}_n$

$$\boldsymbol{G}^T(\boldsymbol{q}_n) = \boldsymbol{Q}_n \cdot \boldsymbol{R}_n = [\boldsymbol{W}_n, \boldsymbol{U}_n] \cdot \begin{bmatrix} \bar{\boldsymbol{R}}_n \\ \mathbf{0}_{(n-m)\times m} \end{bmatrix} \tag{12}$$

containing the nonsingular upper triangular matrix $\bar{\boldsymbol{R}}_n \in \mathbb{R}^{m\times m}$ and the orthogonal matrix $\boldsymbol{Q}_n = [\boldsymbol{W}_n, \boldsymbol{U}_n] \in \mathbb{R}^{n\times n}$ that can be partitioned into the $n \times m$ matrix $\boldsymbol{W}_n$ and the $n \times (n-m)$ matrix $\boldsymbol{U}_n$. Then an implicit representation of the discrete null space matrix is defined by

$$\mathbf{P}(\boldsymbol{q}_n, \boldsymbol{q}_{n+1}) = \big[\boldsymbol{I}_{n\times n} - \boldsymbol{W}_n \cdot \big(\mathbf{G}(\boldsymbol{q}_n, \boldsymbol{q}_{n+1}) \cdot \boldsymbol{W}_n\big)^{-1} \cdot \mathbf{G}(\boldsymbol{q}_n, \boldsymbol{q}_{n+1})\big] \cdot \boldsymbol{U}_n \tag{13}$$

see Part I for a detailed deduction.

Reparametrization of unknowns Similar to the continuous case, a reduction of the system to the minimal possible dimension can be accomplished by a local reparametrization of the constraint manifold in the neighborhood of the discrete configuration variable $\boldsymbol{q}_n \in Q$.

At the time nodes, $\boldsymbol{q}_{n+1}$ is expressed in terms of the incremental generalized coordinates $\boldsymbol{u} \in U \subseteq \mathbb{R}^{n-m}$, such that the constraints are fulfilled:

$$\boldsymbol{F}_{\boldsymbol{q}_n} : U \subseteq \mathbb{R}^{n-m} \to Q \quad \text{i.e.} \quad \boldsymbol{\Phi}(\boldsymbol{q}_{n+1}) = \boldsymbol{\Phi}\left(\boldsymbol{F}_{\boldsymbol{q}_n}(\boldsymbol{u})\right) = \boldsymbol{0}. \tag{14}$$

Insertion of this nodal reparametrization into the d'Alembert-type scheme redundancies $(11)_3$. The resulting d'Alembert-type scheme with nodal reparametrization is equivalent to the constrained scheme (9) (cf. Sect. 3.4. in Part I), thus it also has the key properties of energy–momentum conservation and exact constraint fulfillment. While the constrained scheme becomes increasingly ill-conditioned for decreasing time-steps, the condition number of the d'Alembert-type schemes is independent of the time-step. Altogether the d'Alembert-type scheme with nodal reparametrization features a combination of the required algorithmic conservation properties and the good conditioning quality with a minimal dimension. Inserting $\boldsymbol{v}_{n+1}$ from $(11)_1$ into $(11)_2$, one has to solve a $(n-m)$-dimensional system for $\boldsymbol{u} \in \mathbb{R}^{n-m}$, i.e. the number of equations equals exactly the number of degrees of freedom of the mechanical system (cf. Sect. 3.3. in Part I).

It is worth mentioning that the update of the unknowns within the iterative solution procedure of the nonlinear system of equations (11) can be performed twofold, either in an iterative or in an incremental way. In any case, $\boldsymbol{q}_n = \boldsymbol{F}_{\boldsymbol{q}_n}(\boldsymbol{0})$ holds. Using iterative unknowns, the configuration variable is updated in each iteration of the Newton–Raphson iteration (indexed by l) according to $\boldsymbol{q}_{n+1}^{l+1} = \boldsymbol{F}_{\boldsymbol{q}_{n+1}^{l}}(\boldsymbol{u})$ such that the constraints are fulfilled. On the other hand, a standard additive update of the incremental unknowns $\boldsymbol{u}^{(l)} = \boldsymbol{u}^{(l-1)} + \Delta\boldsymbol{u}^{(l)}$ can be used and the new configuration is determined by $\boldsymbol{q}_{n+1} = \boldsymbol{F}_{\boldsymbol{q}_n}(\boldsymbol{u}^{l_{\max}})$ after the iteration is complete, i.e. $l = l_{\max}$.

3 Dynamics of geometrically exact beams

In the context of structural mechanics, rigid bodies can be considered as a special case of geometrically exact beams, for which the spatial distribution is degenerated to a single point. In the sequel, the discrete null space matrix for the treatment of geometrically exact beams will be deduced.

3.1 Constrained formulation of the equations of motion

The treatment of rigid bodies as structural elements relies on the kinematic assumptions illustrated in Fig. 1 (see [2]) that the placement of a material point relative to an orthonormal

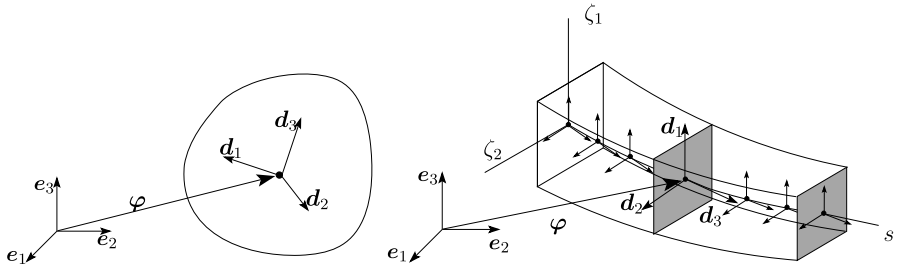

Fig. 1 Configuration of rigid body and a spatially discretized beam

basis $\{\boldsymbol{e}_I\}$ fixed in space can be described as

$$\boldsymbol{x}(\zeta^i, t) = \boldsymbol{\varphi}(t) + \zeta^i \boldsymbol{d}_i(t). \tag{15}$$

Here ζ^i represent coordinates in the body-fixed director triad $\{\boldsymbol{d}_I\}$. Einstein summation convention is used to sum over repeated indices $i = 1, 2, 3$. The time-dependent configuration variable of a rigid body

$$\boldsymbol{q}(t) = \begin{bmatrix} \boldsymbol{\varphi}(t) \\ \boldsymbol{d}_1(t) \\ \boldsymbol{d}_2(t) \\ \boldsymbol{d}_3(t) \end{bmatrix} \in \mathbb{R}^{12} \tag{16}$$

consists of the placement of the center of mass $\boldsymbol{\varphi} \in \mathbb{R}^3$ and the directors $\boldsymbol{d}_I \in \mathbb{R}^3$, $I = 1, 2, 3$ which are assumed to constitute a principal basis for the rigid body. The director triad indicates the rigid body's orientation. The representation of the body's rigidity constrains the directors to stay orthonormal during the motion. This leads to the so-called internal constraints.

This description of a 'one-node structure' can be extended easily to the modeling of geometrically exact beams as special Cosserat continuum (see [2]). The placement of a material point of the beam reads

$$\boldsymbol{x}\left(\zeta^\kappa, s, t\right) = \boldsymbol{\varphi}(s, t) + \zeta^\kappa \boldsymbol{d}_\kappa(s, t). \tag{17}$$

Here $(\zeta^1, \zeta^2, \zeta^3 = s) \in \mathbb{R}^3$ is a triple of curvilinear coordinates with $s \in [0, L] \subset \mathbb{R}$ being the arc-length of the line of centroids $\boldsymbol{\varphi}(s, 0) \in \mathbb{R}^3$ in the reference configuration. $\{\boldsymbol{d}_I\}$ represent an orthonormal triad. The directors $\boldsymbol{d}_\kappa(s, t), \kappa = 1, 2$ span a principal basis of the cross-section at s and time t which is accordingly assumed to stay planar. In the reference configuration, $\boldsymbol{d}_3(s, 0)$ is tangent to the central line $\boldsymbol{\varphi}(s, 0)$ but this is not necessary in a deformed configuration. This allowance of transverse shear deformation corresponds to the Timoshenko beam theory (see [41]). In contrast to the kinematic assumption for the placement of a material point in a rigid body (15), the sum over the repeated index in (17) comprises $\kappa = 1, 2$ and the spatial extension of the beam in the longitudinal direction is accounted for by the parametrization in s. A spatial discretization of the beams configuration (see Fig. 1) in terms of isoparametric finite elements as proposed by [11, 35], using one-dimensional Lagrange-type nodal shape functions $N_\alpha(s)$, reads

$$\boldsymbol{q}^h(s, t) = \sum_{\alpha=1}^{n_{\text{node}}} N_\alpha(s) \boldsymbol{q}^\alpha(t) \in \mathbb{R}^{12} \tag{18}$$

where n_{node} denotes the number of nodes on the central line. This leads to the semi-discrete configuration vector

$$\boldsymbol{q}(t) = \begin{bmatrix} \boldsymbol{q}^1(t) \\ \vdots \\ \boldsymbol{q}^{n_{\text{node}}}(t) \end{bmatrix} \in \mathbb{R}^{12 n_{\text{node}}} \tag{19}$$

where the configuration $\boldsymbol{q}^\alpha$, $\alpha = 1, \ldots, n_{\text{node}}$ at each node takes the form given in (16). Apparently, a spatially discretized beam can be interpreted as a chain of rigid bodies for which the interconnections are prescribed by the connectivity of the spatial finite element method, see e.g. [22]. In the sequel, a rigid body is considered as a special semi-discrete

beam, consisting of only one node, i.e. $n_{\text{node}} = 1$. The internal (orthonormality) constraints $\boldsymbol{\Phi}_{\text{int}} : \mathbb{R}^{12n_{\text{node}}} \to \mathbb{R}^{m_{\text{int}}}$ with $m_{\text{int}} = 6n_{\text{node}}$, pertaining to the underlying continuous theory read for $\alpha = 1, \ldots, n_{\text{node}}$

$$\boldsymbol{\Phi}_{\text{int}}(\boldsymbol{q}) = \begin{bmatrix} \boldsymbol{\Phi}^1_{\text{int}}(\boldsymbol{q}^1) \\ \vdots \\ \boldsymbol{\Phi}^{n_{\text{node}}}_{\text{int}}(\boldsymbol{q}^{n_{\text{node}}}) \end{bmatrix}, \qquad \boldsymbol{\Phi}^{\alpha}_{\text{int}}\big(\boldsymbol{q}^{\alpha}\big) = \begin{bmatrix} [(\boldsymbol{d}^{\alpha}_1)^T \cdot \boldsymbol{d}^{\alpha}_1 - 1]/2 \\ [(\boldsymbol{d}^{\alpha}_2)^T \cdot \boldsymbol{d}^{\alpha}_2 - 1]/2 \\ [(\boldsymbol{d}^{\alpha}_3)^T \cdot \boldsymbol{d}^{\alpha}_3 - 1]/2 \\ (\boldsymbol{d}^{\alpha}_1)^T \cdot \boldsymbol{d}^{\alpha}_2 \\ (\boldsymbol{d}^{\alpha}_1)^T \cdot \boldsymbol{d}^{\alpha}_3 \\ (\boldsymbol{d}^{\alpha}_2)^T \cdot \boldsymbol{d}^{\alpha}_3 \end{bmatrix}. \tag{20}$$

An inherent property of the interpolation (18) is that the constraints on the director triads are relaxed to the nodes of the mesh.

The Jacobian $\boldsymbol{G}_{\text{int}}(\boldsymbol{q}) = D\boldsymbol{\Phi}_{\text{int}}(\boldsymbol{q})$ of the scleronomic holonomic constraints in (20) reads

$$\boldsymbol{G}_{\text{int}}(\boldsymbol{q}) = \begin{bmatrix} \boldsymbol{G}^1_{\text{int}}(\boldsymbol{q}^1) & \boldsymbol{0} & \cdots & \boldsymbol{0} \\ \boldsymbol{0} & \boldsymbol{G}^2_{\text{int}}(\boldsymbol{q}^2) & \cdots & \boldsymbol{0} \\ \vdots & \vdots & \ddots & \vdots \\ \boldsymbol{0} & \boldsymbol{0} & \cdots & \boldsymbol{G}^{n_{\text{node}}}_{\text{int}}(\boldsymbol{q}^{n_{\text{node}}}) \end{bmatrix} \tag{21}$$

with

$$\boldsymbol{G}^{\alpha}_{\text{int}}(\boldsymbol{q}^{\alpha}) = \begin{bmatrix} \boldsymbol{0} & (\boldsymbol{d}^{\alpha}_1)^T & \boldsymbol{0} & \boldsymbol{0} \\ \boldsymbol{0} & \boldsymbol{0} & (\boldsymbol{d}^{\alpha}_2)^T & \boldsymbol{0} \\ \boldsymbol{0} & \boldsymbol{0} & \boldsymbol{0} & (\boldsymbol{d}^{\alpha}_3)^T \\ \boldsymbol{0} & (\boldsymbol{d}^{\alpha}_2)^T & (\boldsymbol{d}^{\alpha}_1)^T & \boldsymbol{0} \\ \boldsymbol{0} & (\boldsymbol{d}^{\alpha}_3)^T & \boldsymbol{0} & (\boldsymbol{d}^{\alpha}_1)^T \\ \boldsymbol{0} & \boldsymbol{0} & (\boldsymbol{d}^{\alpha}_3)^T & (\boldsymbol{d}^{\alpha}_2)^T \end{bmatrix}. \tag{22}$$

Since the internal constraints (20) are quadratic in $\boldsymbol{q}$, the discrete derivative of the constraints coincides with the midpoint evaluation of the constraint Jacobian (21), i.e.

$$\mathbf{G}_{\text{int}}(\boldsymbol{q}_n, \boldsymbol{q}_{n+1}) = \boldsymbol{G}_{\text{int}}(\boldsymbol{q}_{n+\frac{1}{2}}). \tag{23}$$

For the implementation of the constrained scheme, $(9)_1$ is solved for $\boldsymbol{v}_{n+1}$ and inserted into $(9)_2$. For the semi-discrete beam, this leads to a nonlinear system of algebraic equations in terms of $n + m_{\text{int}} = 18n_{\text{node}}$ unknowns.

Remark 3.1 Many current semi-discrete beam formulations avoid the introduction of internal constraints by using rotational degrees of freedom, see e.g. [24, 26]. However it has been shown by Chrisfield and Jelenic [16], that the interpolation of noncommutative finite rotations bears the risk of destroying the objectivity of the strain measures in the semi-discrete model. This can be circumvented by the spatial interpolation of the director triad in (18) as proposed independently in [35] and [11].

Similar to the spatial discretization of the beam's configuration in (18) and (19), the velocities are approximated according to

$$\dot{\boldsymbol{q}}^h(s,t) = \sum_{\alpha=1}^{n_{\text{node}}} N_\alpha(s)\dot{\boldsymbol{q}}^\alpha(t) \in \mathbb{R}^{12} \tag{24}$$

using the semi-discrete velocity vector

$$\dot{\boldsymbol{q}}(t) = \begin{bmatrix} \dot{\boldsymbol{q}}^1(t) \\ \vdots \\ \dot{\boldsymbol{q}}^{n_{\text{node}}}(t) \end{bmatrix} \in \mathbb{R}^{12n_{\text{node}}}. \tag{25}$$

With regard to (16), the velocity vector $\dot{\boldsymbol{q}}^\alpha$, $\alpha = 1, \ldots, n_{\text{node}}$ at each node takes the form

$$\dot{\boldsymbol{q}}^\alpha(t) = \begin{bmatrix} \dot{\boldsymbol{\varphi}}^\alpha(t) \\ \dot{\boldsymbol{d}}_1^\alpha(t) \\ \dot{\boldsymbol{d}}_2^\alpha(t) \\ \dot{\boldsymbol{d}}_3^\alpha(t) \end{bmatrix} \in \mathbb{R}^{12}. \tag{26}$$

Due to the orthonormality of each director triad during the motion and deformation, the director velocities at the nodes can be written as

$$\dot{\boldsymbol{d}}_I^\alpha = \boldsymbol{\omega}^\alpha \times \boldsymbol{d}_I^\alpha = -\widehat{\boldsymbol{d}}_I^\alpha \cdot \boldsymbol{\omega}^\alpha, \quad I = 1, 2, 3 \tag{27}$$

where $\boldsymbol{\omega}^\alpha \in \mathbb{R}^3$ denotes the angular velocity of the triad at the α-th node.

3.2 Discrete null space method with nodal reparametrization

The independent generalized velocities of the semi-discrete beam are given by its twist

$$\boldsymbol{t} = \begin{bmatrix} \boldsymbol{t}^1 \\ \vdots \\ \boldsymbol{t}^{n_{\text{node}}} \end{bmatrix} \in \mathbb{R}^{6n_{\text{node}}} \tag{28}$$

where the twist of the α-th node $\boldsymbol{t}^\alpha \in \mathbb{R}^6$ reads

$$\boldsymbol{t}^\alpha = \begin{bmatrix} \dot{\boldsymbol{\varphi}}^\alpha \\ \boldsymbol{\omega}^\alpha \end{bmatrix} \tag{29}$$

comprising the nodal translational velocity $\dot{\boldsymbol{\varphi}}^\alpha \in \mathbb{R}^3$ and the nodal angular velocity $\boldsymbol{\omega}^\alpha \in \mathbb{R}^3$. Now the redundant velocities $\dot{\boldsymbol{q}} \in \mathbb{R}^{12n_{\text{node}}}$ of the semi-discrete beam may be expressed as $\dot{\boldsymbol{q}} = \boldsymbol{P}_{\text{int}}(\boldsymbol{q}) \cdot \boldsymbol{t}$ where the $12n_{\text{node}} \times 6n_{\text{node}}$ internal null space matrix $\boldsymbol{P}_{\text{int}}(\boldsymbol{q})$ is given by

$$\boldsymbol{P}_{\text{int}}(\boldsymbol{q}) = \begin{bmatrix} \boldsymbol{P}_{\text{int}}^1(\boldsymbol{q}^1) & \boldsymbol{0} & \cdots & \boldsymbol{0} \\ \boldsymbol{0} & \boldsymbol{P}_{\text{int}}^2(\boldsymbol{q}^2) & \cdots & \boldsymbol{0} \\ \vdots & \vdots & \ddots & \vdots \\ \boldsymbol{0} & \boldsymbol{0} & \cdots & \boldsymbol{P}_{\text{int}}^{n_{\text{node}}}(\boldsymbol{q}^{n_{\text{node}}}) \end{bmatrix} \tag{30}$$

and $\boldsymbol{P}^{\alpha}_{\text{int}}(\boldsymbol{q}^{\alpha})$ is the null space matrix associated with the α-th node reading

$$\boldsymbol{P}^{\alpha}_{\text{int}}\left(\boldsymbol{q}^{\alpha}\right) = \begin{bmatrix} \boldsymbol{I} & \boldsymbol{0} \\ \boldsymbol{0} & -\widehat{\boldsymbol{d}}^{\alpha}_{1} \\ \boldsymbol{0} & -\widehat{\boldsymbol{d}}^{\alpha}_{2} \\ \boldsymbol{0} & -\widehat{\boldsymbol{d}}^{\alpha}_{3} \end{bmatrix}. \tag{31}$$

Discrete null space matrix In order to deduce the d'Alembert-type scheme (11), a temporal discrete null space matrix fulfilling (10) must be found. With regard to the midpoint evaluation of the constraint Jacobian in (23), it is evident that a midpoint evaluation of (30) suffices the requirements, i.e.

$$\mathbf{P}_{\text{int}}(\boldsymbol{q}_{n}, \boldsymbol{q}_{n+1}) = \boldsymbol{P}_{\text{int}}(\boldsymbol{q}_{n+\frac{1}{2}}) \tag{32}$$

can be inserted into the d'Alembert-type scheme (11). Solving $(11)_1$ for $\boldsymbol{v}_{n+1}$ and insertion into $(11)_2$ yields $n = 12n_{\text{node}}$ nonlinear algebraic equations for the semi-discrete beam.

Remark 3.2 Note that the coincidence of the discrete derivative of the constraints with the midpoint evaluation of the constraint Jacobian in (23) does not imply that the midpoint evaluation of the continuous null space matrix yields a viable discrete null space matrix in general. This becomes obvious for the treatment of geometrically exact shells in Sect. 4.

Reparametrization of unknowns Due to the $6n_{\text{node}}$ orthonormality constraints (20), the configuration space $\mathbb{R}^{12n_{\text{node}}}$ of the semi-discrete beam is reduced to the constraint manifold

$$Q = \mathbb{R}^{3n_{\text{node}}} \times \left(SO(3)\right)^{n_{\text{node}}} \subset \mathbb{R}^{3n_{\text{node}}} \times \mathbb{R}^{9n_{\text{node}}} \tag{33}$$

where $SO(3)$ is the special orthogonal group. A reduction of the number of unknowns can now be achieved by introducing a rotation matrix $\boldsymbol{R}(\boldsymbol{\theta}^{\alpha}) \in SO(3)$ parametrized in terms of $\boldsymbol{\theta}^{\alpha} \in \mathbb{R}^3$, such that for $\alpha = 1, \ldots, n_{\text{node}}$ and $I = 1, 2, 3$

$$\left(\boldsymbol{d}^{\alpha}_{I}\right)_{n+1} = \boldsymbol{R}\left(\boldsymbol{\theta}^{\alpha}\right) \cdot \left(\boldsymbol{d}^{\alpha}_{I}\right)_{n}. \tag{34}$$

Thus the three rotational variables $\boldsymbol{\theta}^{\alpha} \in \mathbb{R}^3$ play the role of the discrete generalized rotational degrees of freedom (in other words they are incremental rotations) in the time interval $[t_n, t_{n+1}]$ which can be used to express the original nine unknowns associated with the nodal directors $(\boldsymbol{d}^{\alpha}_{I})_{n+1} \in \mathbb{R}^3$, $I = 1, 2, 3$. Concerning the rotation matrix, use is made of the Rodrigues formula, which may be interpreted as a closed-form expression of the exponential map (see e.g. [31]):

$$\boldsymbol{R}(\boldsymbol{\theta}) = \exp(\hat{\boldsymbol{\theta}}) = \boldsymbol{I} + \frac{\sin(\|\boldsymbol{\theta}\|)}{\|\boldsymbol{\theta}\|}\hat{\boldsymbol{\theta}} + \frac{1}{2}\left(\frac{\sin(\|\boldsymbol{\theta}\|/2)}{\|\boldsymbol{\theta}\|/2}\right)^{2}(\hat{\boldsymbol{\theta}})^{2}. \tag{35}$$

When the above reparametrization of unknowns is applied, the new configuration of the semi-discrete beam is specified by $6n_{\text{node}}$ unknowns

$$\boldsymbol{u} = \begin{bmatrix} \boldsymbol{u}^{1} \\ \vdots \\ \boldsymbol{u}^{n_{\text{node}}} \end{bmatrix}, \qquad \boldsymbol{u}^{\alpha} = \left(\boldsymbol{u}^{\alpha}_{\varphi}, \boldsymbol{\theta}^{\alpha}\right) \in U^{\alpha} \subset \mathbb{R}^3 \times \mathbb{R}^3 \tag{36}$$

characterizing the incremental displacement $\boldsymbol{u}_{\varphi}^{\alpha}$ and incremental rotation $\boldsymbol{\theta}^{\alpha}$ in $[t_n, t_{n+1}]$, respectively. Accordingly, in the present case the nodal reparametrization $\boldsymbol{q}_{n+1} = \boldsymbol{F}_{q_n}(\boldsymbol{u}) \in Q$ assumes the form

$$\boldsymbol{q}_{n+1}^{\alpha} = \boldsymbol{F}_{q_n^{\alpha}}^{\alpha}\left(\boldsymbol{u}^{\alpha}\right) = \begin{bmatrix} \boldsymbol{\varphi}_n^{\alpha} + \boldsymbol{u}_{\varphi}^{\alpha} \\ \exp(\widehat{\boldsymbol{\theta}^{\alpha}}) \cdot (\boldsymbol{d}_1^{\alpha})_n \\ \exp(\widehat{\boldsymbol{\theta}^{\alpha}}) \cdot (\boldsymbol{d}_2^{\alpha})_n \\ \exp(\widehat{\boldsymbol{\theta}^{\alpha}}) \cdot (\boldsymbol{d}_3^{\alpha})_n \end{bmatrix}. \tag{37}$$

Insertion of this nodal reparametrization into the d'Alembert-type scheme makes $(11)_3$ redundant and yields the $n - m = 6n_{\text{node}}$-dimensional d'Alembert-type scheme with nodal reparametrization. Note that the present use of rotation matrix (35) is restricted to a single time-step such that possible singularities of (35) are not an issue in practical applications.

4 Dynamics of geometrically exact shells

The present work aims at a specific constrained formulation of nonlinear shells relying on a classical Reissner–Mindlin kinematic. In particular, the starting point is the stress resultant shell model used in Simo et al. [38]. However, in essence the present approach can be directly applied to any degenerate continuum (or continuum-based) C^0 shell element. The shell formulation is based on the three-dimensional continuum theory, where the placement of a material point in the shell reads

$$\boldsymbol{x}\left(\zeta^i, t\right) = \boldsymbol{\varphi}\left(\zeta^1, \zeta^2, t\right) + \zeta \boldsymbol{d}\left(\zeta^1, \zeta^2, t\right) \tag{38}$$

(see Fig. 2). Here $\boldsymbol{\varphi}(\zeta^1, \zeta^2, t)$ denotes the position vector of the actual shell mid-surface labeled with curvilinear coordinates ζ^1, ζ^2. Furthermore, $\zeta^3 = \zeta \in [-h/2, h/2]$ describes the coordinate in the thickness direction $\boldsymbol{d}$, where h is the shell thickness. In the reference configuration, the director $\boldsymbol{d}(\zeta^1, \zeta^2, 0)$ is defined as a unit vector perpendicular to the mid-surface. The director field $\boldsymbol{d}(\zeta^1, \zeta^2, t)$ is assumed to be inextensible and takes into account

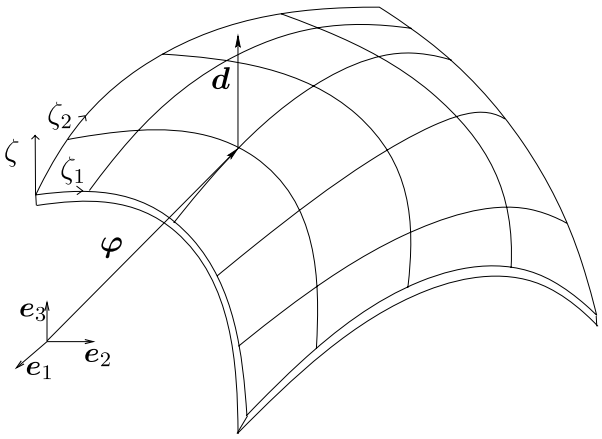

Fig. 2 Configuration of a spatially discretized shell

transverse shearing. The present approach essentially relies on the interpolation of the configuration variable

$$\boldsymbol{q}^h\big(\zeta^1,\zeta^2,t\big)=\sum_{\alpha=1}^{n_{\text{node}}}N_\alpha\big(\zeta^1,\zeta^2\big)\boldsymbol{q}^\alpha(t) \tag{39}$$

where N_α are standard two-dimensional Lagrangean nodal shape functions. Corresponding to (19), the semi-discrete shell configuration vector $\boldsymbol{q}(t)\in\mathbb{R}^{6n_{\text{node}}}$ consists of the nodal configurations

$$\boldsymbol{q}^\alpha(t)=\begin{bmatrix}\boldsymbol{\varphi}^\alpha(t)\\ \boldsymbol{d}^\alpha(t)\end{bmatrix}\in\mathbb{R}^6,\quad \alpha=1,\dots,n_{\text{node}}. \tag{40}$$

Remark 4.1 It is worth mentioning that the director interpolation is a characteristic feature of degenerate shell elements (cf. Büchter and Ramm [14]). In this connection the kinematic assumption of inextensibility is typically imposed directly on the nodal directors by introducing rotational parameters for the unit sphere S^2 (see, for example, Crisfield [15, Sect. 8.2]). An inherent property of the director interpolation in (39) is that the constraints on the director field are relaxed to the nodes of the mesh.

If rotational degrees of freedom are introduced for the description of $\boldsymbol{d}^\alpha\in S^2$, it is natural to make use of nodal angular velocities and accelerations in the design of time-stepping schemes. Representative examples can be found in Simo et al. [38] and Belytschko et al. [4, Sect. 9.5.20]. In contrast to that, the present discretization approach for nonlinear shells does not rely on the use of rotational parameters.

The redundant coordinates (40) have to satisfy the $m_{\text{int}}=n_{\text{node}}$ internal constraints

$$\boldsymbol{\Phi}^\alpha_{\text{int}}\big(\boldsymbol{q}^\alpha\big)=\big[\big(\boldsymbol{d}^\alpha\big)^T\cdot\boldsymbol{d}^\alpha-1\big]/2. \tag{41}$$

The corresponding nodal Jacobians

$$\boldsymbol{G}^\alpha_{\text{int}}\big(\boldsymbol{q}^\alpha\big)=\big[\,\boldsymbol{0}\ \big(\boldsymbol{d}^\alpha\big)^T\,\big] \tag{42}$$

can be inserted into the total Jacobian (21).

Since the internal constraints (41) are quadratic in $\boldsymbol{q}$, the discrete derivative of the constraints coincides with the midpoint evaluation of the constraint Jacobian, consisting of the midpoint evaluation of the nodal Jacobians (42), i.e., (23) holds. For the implementation of the constrained scheme, $(9)_1$ is solved for $\boldsymbol{v}_{n+1}$ and inserted into $(9)_2$. For the semi-discrete shell, this leads to a nonlinear system of algebraic equations in terms of $n+m_{\text{int}}=7n_{\text{node}}$ unknowns.

Corresponding to (24), the temporal differentiation of (39) involves the nodal velocity vectors

$$\dot{\boldsymbol{q}}^\alpha(t)=\begin{bmatrix}\dot{\boldsymbol{\varphi}}^\alpha(t)\\ \dot{\boldsymbol{d}}^\alpha(t)\end{bmatrix}\in\mathbb{R}^6. \tag{43}$$

Due to the inextensibility of the director field, each nodal director velocity $\dot{\boldsymbol{d}}^\alpha$ is restricted to the two-dimensional tangent space $T_{\boldsymbol{d}^\alpha}S^2$, i.e.,

$$\dot{\boldsymbol{d}}^\alpha=\dot\theta^\alpha_1\boldsymbol{d}^\alpha_1+\dot\theta^\alpha_2\boldsymbol{d}^\alpha_2 \tag{44}$$

where $\boldsymbol{d}_1^\alpha$, $\boldsymbol{d}_2^\alpha$ span an orthonormal basis for this tangent space such that $\boldsymbol{d}_1^\alpha$, $\boldsymbol{d}_2^\alpha$, $\boldsymbol{d}^\alpha$ are mutually orthonormal vectors. Consequently $\dot{\boldsymbol{d}}^\alpha$ can be written in the form (27), with the difference that for the shell the nodal angular velocity reads

$$\boldsymbol{\omega}^\alpha = -\dot{\theta}_2^\alpha \boldsymbol{d}_1^\alpha + \dot{\theta}_1^\alpha \boldsymbol{d}_2^\alpha. \tag{45}$$

4.1 Discrete null space method with nodal reparametrization

The independent generalized velocities of the semi-discrete shell are given by

$$\boldsymbol{s} = \begin{bmatrix} \boldsymbol{s}^1 \\ \vdots \\ \boldsymbol{s}^{n_{\text{node}}} \end{bmatrix} \in \mathbb{R}^{5n_{\text{node}}} \tag{46}$$

where the independent generalized velocities of the α-th node $\boldsymbol{s}^\alpha \in \mathbb{R}^5$ read

$$\boldsymbol{s}^\alpha = \begin{bmatrix} \dot{\boldsymbol{\varphi}}^\alpha \\ \dot{\theta}_1^\alpha \\ \dot{\theta}_2^\alpha \end{bmatrix} \tag{47}$$

comprising the nodal translational velocity $\dot{\boldsymbol{\varphi}}^\alpha \in \mathbb{R}^3$ and the coordinates $\dot{\theta}_1^\alpha$, $\dot{\theta}_2^\alpha$ of the nodal director velocity given in (44). Now the redundant velocities $\dot{\boldsymbol{q}} \in \mathbb{R}^{6n_{\text{node}}}$ of the semi-discrete shell may be expressed as $\dot{\boldsymbol{q}} = \boldsymbol{P}_{\text{int}}(\boldsymbol{q}) \cdot \boldsymbol{s}$ where the $6n_{\text{node}} \times 5n_{\text{node}}$ internal null space matrix of the form (30) comprises the null space matrices associated with the α-th node $\boldsymbol{P}_{\text{int}}^\alpha(\boldsymbol{q}^\alpha)$ reading

$$\boldsymbol{P}_{\text{int}}^\alpha(\boldsymbol{q}^\alpha) = \begin{bmatrix} \boldsymbol{I} & \boldsymbol{0}_{3\times1} & \boldsymbol{0}_{3\times1} \\ \boldsymbol{0}_{3\times3} & \boldsymbol{d}_1^\alpha & \boldsymbol{d}_2^\alpha \end{bmatrix}. \tag{48}$$

Discrete null space matrix With regard to condition (10), it can be easily verified that a proper choice of the discrete null space matrix comprises the 6×5 nodal submatrices

$$\mathbf{P}_{\text{int}}^\alpha\left(\boldsymbol{q}_n^\alpha, \boldsymbol{q}_{n+1}^\alpha\right) = \begin{bmatrix} \boldsymbol{I} & \boldsymbol{0}_{3\times1} & \boldsymbol{0}_{3\times1} \\ \boldsymbol{0}_{3\times3} & \widetilde{\boldsymbol{d}}_1^\alpha & \widetilde{\boldsymbol{d}}_2^\alpha \end{bmatrix} \tag{49}$$

where for $\kappa = 1, 2$

$$\widetilde{\boldsymbol{d}}_\kappa^\alpha = \left(\boldsymbol{d}_\kappa^\alpha\right)_n - \frac{\left(\boldsymbol{d}_\kappa^\alpha\right)_n^T \cdot \boldsymbol{d}_{n+\frac{1}{2}}^\alpha}{\left(\boldsymbol{d}^\alpha\right)_n^T \cdot \boldsymbol{d}_{n+\frac{1}{2}}^\alpha} \boldsymbol{d}_n^\alpha. \tag{50}$$

The assembly of the submatrices given in (49) yields the total null space matrix pertaining to the internal inextensibility constraints for the shell director field, which can be inserted into the d'Alembert-type scheme (11). Solving $(11)_1$ for $\boldsymbol{v}_{n+1}$ and insertion into $(11)_2$ yields $n = 6n_{\text{node}}$ nonlinear algebraic equations for the semi-discrete shell.

Reparametrization of unknowns Due to the n_{node} inextensibility constraints (41), the configuration space $\mathbb{R}^{6n_{\text{node}}}$ of the semi-discrete shell is reduced to the constraint manifold

$$Q = \mathbb{R}^{3n_{\text{node}}} \times \left(S^2\right)^{n_{\text{node}}} \subset \mathbb{R}^{3n_{\text{node}}} \times \mathbb{R}^{3n_{\text{node}}}. \tag{51}$$

A further size-reduction of the algebraic system to be solved can be achieved by introducing new incremental unknowns $\boldsymbol{u} \in U \subset \mathbb{R}^{5n_{\text{node}}}$ via a reparametrization of the form (14). The new nodal configuration of the semi-discrete shell is specified by 5 unknowns

$$\boldsymbol{u}^{\alpha} = \left(\boldsymbol{u}_{\varphi}^{\alpha}, \theta_1^{\alpha}, \theta_2^{\alpha}\right) \in U^{\alpha} \subset \mathbb{R}^3 \times \mathbb{R}^2 \tag{52}$$

characterizing the incremental displacement $\boldsymbol{u}_{\varphi}^{\alpha}$ and incremental rotational parameters $[\theta_1^{\alpha}, \theta_2^{\alpha}]^T = \boldsymbol{\theta}^{\alpha}$ parametrizing the unit sphere. Similar to (37), in the present case the nodal reparametrization assumes the form

$$\boldsymbol{q}_{n+1}^{\alpha} = \boldsymbol{F}_{q_n^{\alpha}}^{\alpha}\left(\boldsymbol{u}^{\alpha}\right) = \begin{bmatrix} \boldsymbol{\varphi}_n^{\alpha} + \boldsymbol{u}_{\varphi}^{\alpha} \\ \exp_{d_n^{\alpha}}\left(\boldsymbol{D}^{\alpha}(\boldsymbol{q}_n^{\alpha}) \cdot \boldsymbol{\theta}^{\alpha}\right) \end{bmatrix} \tag{53}$$

with the 3×2 matrix $\boldsymbol{D}^{\alpha}(\boldsymbol{q}_n^{\alpha}) = [\,(\boldsymbol{d}_1^{\alpha})_n \;\; (\boldsymbol{d}_2^{\alpha})_n\,]$ and the following form of the exponential map $\exp_{d_n^{\alpha}} : T_{d_n^{\alpha}} S^2 \to S^2$

$$\exp_{d_n^{\alpha}}\left(\boldsymbol{D}^{\alpha}\left(\boldsymbol{q}_n^{\alpha}\right) \cdot \boldsymbol{\theta}^{\alpha}\right) = \cos\left(\left\|\boldsymbol{D}^{\alpha}\left(\boldsymbol{q}_n^{\alpha}\right) \cdot \boldsymbol{\theta}^{\alpha}\right\|\right)\boldsymbol{d}_n^{\alpha} + \frac{\sin(\|\boldsymbol{D}^{\alpha}\left(\boldsymbol{q}_n^{\alpha}\right) \cdot \boldsymbol{\theta}^{\alpha}\|)}{\|\boldsymbol{D}^{\alpha}(\boldsymbol{q}_n^{\alpha}) \cdot \boldsymbol{\theta}^{\alpha}\|}\boldsymbol{D}^{\alpha}(\boldsymbol{q}_n^{\alpha}) \cdot \boldsymbol{\theta}^{\alpha}. \tag{54}$$

With this reparametrization at hand, the $n - m_{\text{int}} = 5n_{\text{node}}$-dimensional d'Alembert-type scheme with nodal reparametrization for the semi-discrete shell can be derived.

5 Flexible multibody system dynamics

The description of rigid bodies and spatially discretized geometrically exact beams and shells as constrained continua in terms of the configuration variables given in (16), (19) and (40) respectively allows their coupling to a multibody system consisting of rigid and elastic components in a systematic way. As a generalization of (19), the configuration vectors of all components in the multibody system are combined into the general configuration vector $\boldsymbol{q}(t) \in \mathbb{R}^n$ where n is a multiple of the actual number of spatial nodes present in the semi-discrete system. Besides the internal constraints pertaining to the kinematic assumptions of the specific structural element, the configuration vector of the total multibody system is subject to 'external constraints' $\boldsymbol{\Phi}_{\text{ext}} : \mathbb{R}^n \to \mathbb{R}^{m_{\text{ext}}}$. These represent a reduction of the degrees of freedom of the total multibody system imposed by kinematic restrictions from the outset and can be classified in Table 1.

As a consequence of the uniform description of all multibody components by means of the DAEs (2), the external constraint functions arising in the described cases are at most

Table 1 Different types of external constraints

1	Neighboring components may be coupled by various types of joints $J \in \{R, P, C, S, E\}$. The coupling reduces the relative motion of the components to the $r^{(J)}$ joint velocities $\boldsymbol{\tau}^{(J)}$ (see Table 2).
2	In the case of intersections of shells and/or beams, a rigid connection between the adjacent components is assumed. In this case, the common nodes have three translational and three rotational degrees of freedom, see e.g. [23, 37].
3	Standard Dirichlet boundary conditions can be imposed as external constraints.

Table 2 Different types of joints for lower kinematic pairs with corresponding number of external constraints $m_{\text{ext}}^{(J)}$ and number or relative degrees of freedom $r^{(J)}$

	Revolute (R)	Prismatic (P)	Cylindrical (C)	Spherical (S)	Planar (E)
$m_{\text{ext}}^{(J)}$	5	5	4	3	3
$r^{(J)}$	1	1	2	3	3

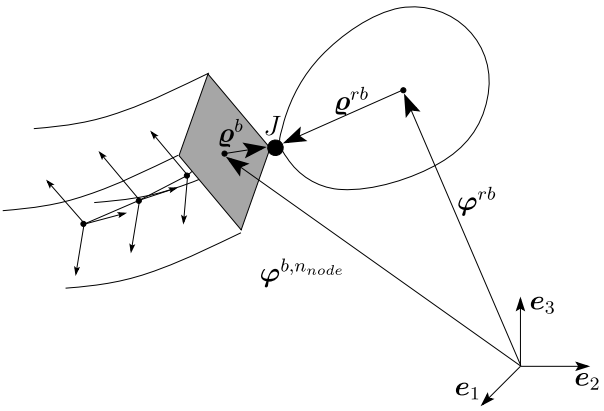

Fig. 3 Coupling of a beam to a rigid body

quadratic. This property simplifies the construction of a discrete null space matrix fulfilling (10), since the discrete derivative of the corresponding external constraints coincides with the midpoint evaluation of the continuous constraint Jacobian, i.e., (23) holds.

The application of the discrete null space method to the dynamics of multibody systems comprised by rigid bodies interconnected by the joints listed in Table 2 is explained in Part II. In particular, a systematic design of discrete null space matrices pertaining to lower kinematic pairs is proposed there.

Three examples of multibody systems comprising elastic components are given in the sequel before the general procedure for the treatment of arbitrary multibody systems by the discrete null space method is outlined in Sect. 5.1.

Example 5.1 (Coupling of a beam to a rigid body)

The configuration variable of the multibody system in Fig. 3 reads

$$\boldsymbol{q}(t) = \begin{bmatrix} \boldsymbol{q}^{1}(t) \\ \vdots \\ \boldsymbol{q}^{n_{\text{node}}}(t) \\ \boldsymbol{q}^{rb}(t) \end{bmatrix} \in \mathbb{R}^{12(n_{\text{node}}+1)}. \tag{55}$$

It is subject to the internal constraints of the form (20) and the external constraints representing the coupling by a specific joint explained in Part II. Interconnecting the last beam node to a rigid body by means of a specific joint $J \in \{R, P, C, S, E\}$, for example, reduces the relative motion of the rigid body with respect to the beam to the $r^{(J)}$ joint velocities $\boldsymbol{\tau}^{(J)}$ (see Table 2). The motion of the multibody system is characterized by the independent

generalized velocities $\boldsymbol{v} \in \mathbb{R}^{6n_{\text{node}}+r^{(J)}}$ with

$$\boldsymbol{v} = \begin{bmatrix} \boldsymbol{t}^1 \\ \vdots \\ \boldsymbol{t}^{n_{\text{node}}} \\ \boldsymbol{\tau}^{(J)} \end{bmatrix}. \tag{56}$$

The $12(n_{\text{node}}+1)$-dimensional redundant velocity vector of the multibody system can then be expressed via

$$\dot{\boldsymbol{q}} = \boldsymbol{P}(\boldsymbol{q}) \cdot \boldsymbol{v} = \boldsymbol{P}_{\text{int}}(\boldsymbol{q}) \cdot \boldsymbol{P}_{\text{ext}}(\boldsymbol{q}) \cdot \boldsymbol{v}. \tag{57}$$

The $12(n_{\text{node}}+1) \times 6(n_{\text{node}}+1)$ internal null space matrix is given by

$$\boldsymbol{P}_{\text{int}}(\boldsymbol{q}) = \begin{bmatrix} \boldsymbol{P}^1_{\text{int}}(\boldsymbol{q}^1) & \boldsymbol{0} & \cdots & \boldsymbol{0} & \boldsymbol{0} \\ \boldsymbol{0} & \boldsymbol{P}^2_{\text{int}}(\boldsymbol{q}^2) & \cdots & \boldsymbol{0} & \boldsymbol{0} \\ \vdots & \vdots & \ddots & \vdots & \vdots \\ \boldsymbol{0} & \boldsymbol{0} & \cdots & \boldsymbol{P}^{n_{\text{node}}}_{\text{int}}(\boldsymbol{q}^{n_{\text{node}}}) & \boldsymbol{0} \\ \boldsymbol{0} & \boldsymbol{0} & \cdots & \boldsymbol{0} & \boldsymbol{P}^{rb}_{\text{int}}(\boldsymbol{q}^{rb}) \end{bmatrix} \tag{58}$$

with $\boldsymbol{P}^{\alpha}_{\text{int}}(\boldsymbol{q}^{\alpha})$ given in (31) for $\alpha = 1, \ldots, n_{\text{node}}, rb$ and $\boldsymbol{0}$ denoting the 12×6 zero matrix. From the treatment of kinematic pairs in Part II, it can be inferred that the $6(n_{\text{node}}+1) \times (6n_{\text{node}} + r^{(J)})$ external null space matrix $\boldsymbol{P}_{\text{ext}}(\boldsymbol{q})$ reads

$$\boldsymbol{P}_{\text{ext}}(\boldsymbol{q}) = \begin{bmatrix} \boldsymbol{I} & \boldsymbol{0} & \cdots & \boldsymbol{0} & \boldsymbol{0}_{6\times r^{(J)}} \\ \boldsymbol{0} & \boldsymbol{I} & \cdots & \boldsymbol{0} & \boldsymbol{0}_{6\times r^{(J)}} \\ \vdots & \vdots & \ddots & \vdots & \vdots \\ \boldsymbol{0} & \boldsymbol{0} & \cdots & \boldsymbol{I} & \boldsymbol{0}_{6\times r^{(J)}} \\ \boldsymbol{0} & \boldsymbol{0} & \cdots & \boldsymbol{P}^{2,(J)}_{\text{ext}}(\boldsymbol{q}) & \end{bmatrix}. \tag{59}$$

Here $\boldsymbol{I}$ and $\boldsymbol{0}$ denote the 6×6 identity and zero matrices respectively. Different forms of the external null space matrix $\boldsymbol{P}^{2,(J)}_{\text{ext}}(\boldsymbol{q})$ accounting for specific joints are given explicitly in Part II.

Example 5.2 (Rigid connection of two beams) A rigid connection between the node $b_1 \in \{1, \ldots, n^1_{\text{node}}\}$ with nodal configuration vector $\boldsymbol{q}^{1,b_1} \in \mathbb{R}^{12}$ in the first beam (which contains n^1_{node} nodes) and the node $b_2 \in \{1, \ldots, n^2_{\text{node}}\}$ with nodal configuration vector $\boldsymbol{q}^{2,b_2}$ in the second beam (which contains n^2_{node} nodes) gives rise to the following six constraint functions

$$\boldsymbol{\Phi}^{(F)}_{\text{ext}}(\boldsymbol{q}) = \begin{bmatrix} \boldsymbol{\varphi}^{2,b_2} - \boldsymbol{\varphi}^{1,b_1} + \boldsymbol{\varrho}^{b_2} - \boldsymbol{\varrho}^{b_1} \\ (\boldsymbol{d}^{1,b_1}_1)^T \cdot \boldsymbol{d}^{2,b_2}_2 - \eta_1 \\ (\boldsymbol{d}^{1,b_1}_2)^T \cdot \boldsymbol{d}^{2,b_2}_3 - \eta_2 \\ (\boldsymbol{d}^{1,b_1}_3)^T \cdot \boldsymbol{d}^{2,b_2}_1 - \eta_3 \end{bmatrix} \tag{60}$$

where $\boldsymbol{\varrho}^{b_1}$ and $\boldsymbol{\varrho}^{b_2}$ point from $\boldsymbol{\varphi}^{1,b_1}$ respectively $\boldsymbol{\varphi}^{2,b_2}$ to the rigidly connected point and η_1, η_2, η_3 are constant and need to be consistent with the initial conditions. Thus there are

no relative degrees of freedom of the node b_2 with respect to the node b_1, and its twist can be calculated in terms of the twist of the node b_1 via

$$\boldsymbol{t}^{2,b_2} = \boldsymbol{P}_{\text{ext}}^{2,(F)}(\boldsymbol{q}) \cdot \boldsymbol{t}^{1,b_1} \tag{61}$$

with the 6×6 null space matrix pertaining to the rigid connection

$$\boldsymbol{P}_{\text{ext}}^{2,(F)}(\boldsymbol{q}) = \begin{bmatrix} \boldsymbol{I} & \widehat{\boldsymbol{\varrho}^{b_2} - \boldsymbol{\varrho}^{b_1}} \\ \boldsymbol{0} & \boldsymbol{I} \end{bmatrix}. \tag{62}$$

Then the mapping $\boldsymbol{t} = \boldsymbol{P}_{\text{ext}}(\boldsymbol{q}) \cdot \boldsymbol{v}$ of the independent generalized velocities $\boldsymbol{v} \in \mathbb{R}^{6(n^1_{\text{node}}+n^2_{\text{node}}-1)}$ to the twist of the multibody system $\boldsymbol{t} \in \mathbb{R}^{6(n^1_{\text{node}}+n^2_{\text{node}})}$ via the external null space matrix $\boldsymbol{P}_{\text{ext}}(\boldsymbol{q})$ reads explicitly

$$\begin{bmatrix} \boldsymbol{t}^{1,1} \\ \vdots \\ \boldsymbol{t}^{1,b_1} \\ \vdots \\ \boldsymbol{t}^{1,n^1_{\text{node}}} \\ \boldsymbol{t}^{2,1} \\ \vdots \\ \boldsymbol{t}^{2,b_2} \\ \vdots \\ \boldsymbol{t}^{2,n^2_{\text{node}}} \end{bmatrix} = \begin{bmatrix} \boldsymbol{I} & \cdots & \boldsymbol{0} & \cdots & \boldsymbol{0} & \boldsymbol{0} & \cdots & \boldsymbol{0} & \boldsymbol{0} & \cdots & \boldsymbol{0} \\ \vdots & \ddots & \vdots & \ddots & \vdots & \vdots & \ddots & \vdots & \vdots & \ddots & \vdots \\ \boldsymbol{0} & \cdots & \boldsymbol{I} & \cdots & \boldsymbol{0} & \boldsymbol{0} & \cdots & \boldsymbol{0} & \boldsymbol{0} & \cdots & \boldsymbol{0} \\ \vdots & \ddots & \vdots & \ddots & \vdots & \vdots & \ddots & \vdots & \vdots & \ddots & \vdots \\ \boldsymbol{0} & \cdots & \boldsymbol{0} & \cdots & \boldsymbol{I} & \boldsymbol{0} & \cdots & \boldsymbol{0} & \boldsymbol{0} & \cdots & \boldsymbol{0} \\ \boldsymbol{0} & \cdots & \boldsymbol{0} & \cdots & \boldsymbol{0} & \boldsymbol{I} & \cdots & \boldsymbol{0} & \boldsymbol{0} & \cdots & \boldsymbol{0} \\ \vdots & \ddots & \vdots & \ddots & \vdots & \vdots & \ddots & \vdots & \vdots & \ddots & \vdots \\ \boldsymbol{0} & \cdots & \boldsymbol{P}_{\text{ext}}^{2,(F)} & \cdots & \boldsymbol{0} & \boldsymbol{0} & \cdots & \boldsymbol{0} & \boldsymbol{0} & \cdots & \boldsymbol{0} \\ \vdots & \ddots & \vdots & \ddots & \vdots & \vdots & \ddots & \vdots & \vdots & \ddots & \vdots \\ \boldsymbol{0} & \cdots & \boldsymbol{0} & \cdots & \boldsymbol{0} & \boldsymbol{0} & \cdots & \boldsymbol{0} & \boldsymbol{0} & \cdots & \boldsymbol{I} \end{bmatrix} \cdot \begin{bmatrix} \boldsymbol{t}^{1,1} \\ \vdots \\ \boldsymbol{t}^{1,b_1} \\ \vdots \\ \boldsymbol{t}^{1,n^1_{\text{node}}} \\ \boldsymbol{t}^{2,1} \\ \vdots \\ \boldsymbol{t}^{2,b_2-1} \\ \boldsymbol{t}^{2,b_2+1} \\ \vdots \\ \boldsymbol{t}^{2,n^2_{\text{node}}} \end{bmatrix}. \tag{63}$$

Example 5.3 (Shell intersection)

In the case of shell intersections, a rigid connection between the adjacent shells is assumed, see e.g. [23, 37]. Let the node α_1 with nodal configuration vector $\boldsymbol{q}^{\alpha_1} \in \mathbb{R}^6$ in the first shell be rigidly connected to the node α_2 with nodal configuration vector $\boldsymbol{q}^{\alpha_2}$ in the second shell. In contrast to the rigid connection of beams described in Example 5.2, here the rigid connection points coincide with nodes in the mesh of the semi-discrete shells. Then the intersection gives rise to the following external constraint function

$$\boldsymbol{\Phi}_{\text{ext}}^{(I)}(\boldsymbol{q}) = \begin{bmatrix} \boldsymbol{\varphi}^{\alpha_2} - \boldsymbol{\varphi}^{\alpha_1} \\ (\boldsymbol{d}^{\alpha_1})^T \cdot \boldsymbol{d}^{\alpha_2} - \eta \end{bmatrix} \tag{64}$$

where $\eta = \cos\beta_0$ and β_0 is the angle between $\boldsymbol{d}^{\alpha_1}$ and $\boldsymbol{d}^{\alpha_2}$ in the initial configuration. Consequently, only $r^{(I)} = 1$ rotational degree of freedom characterizes the motion of node α_2 relative to node α_1. Altogether the 'shared' node has three translational and three rotational degrees of freedom and the corresponding velocities can be combined into the translational velocity $\dot{\boldsymbol{\varphi}}^{\alpha_1}$ and the angular velocity $\boldsymbol{\omega}$. According to (45), the angular velocity must fulfill

$$\begin{aligned} \dot{\theta}_1^{\alpha_1} &= \left(\boldsymbol{d}_2^{\alpha_1}\right)^T \cdot \boldsymbol{\omega}, \qquad & \dot{\theta}_2^{\alpha_1} &= -\left(\boldsymbol{d}_1^{\alpha_1}\right)^T \cdot \boldsymbol{\omega}, \\ \dot{\theta}_1^{\alpha_2} &= \left(\boldsymbol{d}_2^{\alpha_2}\right)^T \cdot \boldsymbol{\omega}, \qquad & \dot{\theta}_2^{\alpha_2} &= -\left(\boldsymbol{d}_1^{\alpha_2}\right)^T \cdot \boldsymbol{\omega}. \end{aligned} \tag{65}$$

Now the redundant velocities $\dot{\boldsymbol{q}}^{\alpha_\kappa}$ are reduced in two steps. First, the internal constraints yield $\dot{\boldsymbol{q}}^{\alpha_\kappa} = \boldsymbol{P}_{\text{int}}^{\alpha_\kappa}(\boldsymbol{q}^{\alpha_\kappa}) \cdot \boldsymbol{s}^{\alpha_\kappa}$ for $\kappa = 1, 2$, with the internal null space matrix given in (48). The second step involves the 5×6 partial external null space matrix

$$\boldsymbol{P}_{\text{ext}}^{(I)_{\alpha_\kappa}}\left(\boldsymbol{q}^{\alpha_\kappa}\right) = \begin{bmatrix} \boldsymbol{I} & \boldsymbol{0}_{3\times 3} \\ \boldsymbol{0}_{1\times 3} & (\boldsymbol{d}_2^{\alpha_\kappa})^T \\ \boldsymbol{0}_{1\times 3} & -(\boldsymbol{d}_1^{\alpha_\kappa})^T \end{bmatrix}. \tag{66}$$

With regard to (65), the following relation holds

$$\boldsymbol{s}^{\alpha_\kappa} = \boldsymbol{P}_{\text{ext}}^{(I)_{\alpha_\kappa}}\left(\boldsymbol{q}^{\alpha_\kappa}\right) \cdot \begin{bmatrix} \dot{\boldsymbol{\varphi}}^{\alpha_1} \\ \boldsymbol{\omega} \end{bmatrix}. \tag{67}$$

Finally, the external null space matrices pertaining to the nodes α_1, α_2 in the shell intersection read

$$\boldsymbol{P}^{(I)_{\alpha_\kappa}}\left(\boldsymbol{q}^{\alpha_\kappa}\right) = \boldsymbol{P}_{\text{int}}^{\alpha_\kappa}\left(\boldsymbol{q}^{\alpha_\kappa}\right) \cdot \boldsymbol{P}_{\text{ext}}^{(I)_{\alpha_\kappa}}\left(\boldsymbol{q}^{\alpha_\kappa}\right) = \begin{bmatrix} \boldsymbol{I} & \boldsymbol{0} \\ \boldsymbol{0} & -\widehat{\boldsymbol{d}^{\alpha_\kappa}} \end{bmatrix}. \tag{68}$$

5.1 General treatment by the discrete null space method

A generalization to arbitrary multibody systems consisting of several elastic and rigid components can be accomplished in a straightforward way. Specific nodal configuration vectors $\boldsymbol{q}^{\alpha}, \boldsymbol{q}^{\beta}$ are coupled according to the procedure described for kinematic pairs, regardless whether they represent a node in a spatially discretized beam, shell or a rigid body's configuration. The order in which the nodal configuration vectors are combined to the configuration vector of the multibody system (see e.g., (55)), defines the positions of the node-specific block-matrices in the internal null space matrix (see e.g., (58)). It also prescribes the assembly of the external null space matrices representing specific couplings in the total external null space matrix (see e.g., (59) and (63)).

A general procedure for the treatment of multibody systems consisting of rigid and elastic components by the discrete null space method comprises the steps described in Table 3. All alternatives for the construction of the discrete null space matrix in step (iii) yield equivalent results, but they differ significantly in the arising computational costs. From the computational point of view, the explicit representation in **alternative iii.1** is most desirable. If it is not feasible for the problem at hand (e.g., for most closed loop systems) the semi-explicit representation in **alternative iii.3** states a reasonable compromise while the implicit representation in **alternative iii.2** requires the highest computational costs.

5.2 Numerical example: spatial slider-crank mechanism

The multibody system under consideration is a three-dimensional slider-crank mechanism. The initial configuration is depicted in Fig. 4. It consists of a horizontal elastic beam of length 6, which is discretized by 20 linear beam elements and characterized by the axial and shear stiffness $EA = GA = 10^5$ and bending and torsional stiffness $EI = EJ = 10^4$. The middle node (node 11) is rigidly connected (see Example 5.2) to the first node of the elastic slider of length 4, which is discretized by 15 linear beam elements and characterized by the axial and shear stiffness $EA = GA = 10^6$ and bending and torsional stiffness $EI = EJ = 10^5$. Assuming that the hyperelastic material behavior of the beams is governed

Table 3 General procedure for the treatment of flexible multibody systems by the discrete null space method

(i) definition of the order in which the nodal configuration variables (regardless whether they represent a node in a spatially discretized beam, shell or a rigid body's configuration) are combined to the configuration variable of the multibody system $\boldsymbol{q} \in \mathbb{R}^n$

(ii) identification of independent constraint functions and full-rank Jacobian comprising m_{int} internal constraint functions and m_{ext} external constraint functions corresponding to n_c couplings or bearings

$$\boldsymbol{g}(\boldsymbol{q}) = \begin{bmatrix} \boldsymbol{g}_{\text{int}}(\boldsymbol{q}) \\ \boldsymbol{g}^1_{\text{ext}}(\boldsymbol{q}) \\ \vdots \\ \boldsymbol{g}^{n_c}_{\text{ext}}(\boldsymbol{q}) \end{bmatrix} \in \mathbb{R}^m, \qquad \boldsymbol{G}(\boldsymbol{q}) = \begin{bmatrix} \boldsymbol{G}_{\text{int}}(\boldsymbol{q}) \\ \boldsymbol{G}^1_{\text{ext}}(\boldsymbol{q}) \\ \vdots \\ \boldsymbol{G}^{n_c}_{\text{ext}}(\boldsymbol{q}) \end{bmatrix} \in \mathbb{R}^{m \times n}$$

where $m = m_{\text{int}} + m_{\text{ext}} = m_{\text{int}} + m^1_{\text{ext}} + \cdots + m^{n_c}_{\text{ext}}$

(iii) construction of a full-rank discrete null space matrix $\mathbf{P}(\boldsymbol{q}_n, \boldsymbol{q}_{n+1}) \in \mathbb{R}^{n \times (n-m)}$ fulfilling $\mathbf{G}(\boldsymbol{q}_n, \boldsymbol{q}_{n+1}) \cdot \mathbf{P}(\boldsymbol{q}_n, \boldsymbol{q}_{n+1}) = \mathbf{0}$ by employing one of the alternatives outlined in the sequel

alternative iii.1 (explicit representation)
construction of a continuous null space matrix $\boldsymbol{P}(\boldsymbol{q}) \in \mathbb{R}^{n \times (n-m)}$ fulfilling $\boldsymbol{G}(\boldsymbol{q}) \cdot \boldsymbol{P}(\boldsymbol{q}) = \mathbf{0}$ by (a) or (b)

(a) velocity analysis (see (57)): successive reduction of the redundant velocities $\dot{\boldsymbol{q}} \in \mathbb{R}^n$ to the independent generalized velocities $\boldsymbol{v} \in \mathbb{R}^{n-m}$
- internal constraints: $\dot{\boldsymbol{q}} = \boldsymbol{P}_{\text{int}}(\boldsymbol{q}) \cdot \boldsymbol{v}_{\text{int}}, \quad \boldsymbol{v}_{\text{int}} \in \mathbb{R}^{n-m_{\text{int}}}$
  the order in which the nodal independent generalized velocities $\boldsymbol{t}^\alpha, \boldsymbol{s}^\alpha$ are combined in $\boldsymbol{v}_{\text{int}}$ is defined by that of the total configuration variable specified in step (i)
- first external coupling or bearing:
  $\dot{\boldsymbol{q}} = \boldsymbol{P}_{\text{int}}(\boldsymbol{q}) \cdot \boldsymbol{P}^1_{\text{ext}}(\boldsymbol{q}) \cdot \boldsymbol{v}^1, \quad \boldsymbol{v}^1 \in \mathbb{R}^{n-m_{\text{int}}-m^1_{\text{ext}}}$
  $\vdots$
- last external coupling or bearing:
  $\dot{\boldsymbol{q}} = \boldsymbol{P}_{\text{int}}(\boldsymbol{q}) \cdot \boldsymbol{P}^1_{\text{ext}}(\boldsymbol{q}) \cdot \cdots \cdot \boldsymbol{P}^{n_c}_{\text{ext}}(\boldsymbol{q}) \cdot \boldsymbol{v}, \ \boldsymbol{v} \in \mathbb{R}^{n-m}$
- $\boldsymbol{P}(\boldsymbol{q}) = \boldsymbol{P}_{\text{int}}(\boldsymbol{q}) \cdot \boldsymbol{P}^1_{\text{ext}}(\boldsymbol{q}) \cdot \cdots \cdot \boldsymbol{P}^{n_c}_{\text{ext}}(\boldsymbol{q})$

(b) explicit analytical QR-decomposition of the transposed constraint Jacobian in terms of $\boldsymbol{q}$: $\boldsymbol{G}^T = [\boldsymbol{Q}_1, \boldsymbol{Q}_2] \cdot \boldsymbol{R}$ yields $\boldsymbol{P}(\boldsymbol{q}) = \boldsymbol{Q}_2(\boldsymbol{q})$ (see (8))

midpoint evaluation of the continuous null space matrix $\boldsymbol{P}(\boldsymbol{q}_{n+\frac{1}{2}})$ or slight modification of the midpoint evaluation yields $\mathbf{P}(\boldsymbol{q}_n, \boldsymbol{q}_{n+1})$ (see Part II)

alternative iii.2 (implicit representation)
QR-decomposition of $\boldsymbol{G}^T(\boldsymbol{q}_n)$ yields the necessary submatrices to infer $\mathbf{P}(\boldsymbol{q}_n, \boldsymbol{q}_{n+1})$ via formula (13)

alternative iii.3 (semi-explicit representation)

- explicit representation of internal discrete null space matrix:
  $\mathbf{P}_{\text{int}}(\boldsymbol{q}_n, \boldsymbol{q}_{n+1}) = \boldsymbol{P}_{\text{int}}(\boldsymbol{q}_{n+\frac{1}{2}})$
- if possible: $\mathbf{P}^c_{\text{ext}}(\boldsymbol{q}_n, \boldsymbol{q}_{n+1})$ is obtained explicitly by midpoint evaluation $\boldsymbol{P}^c_{\text{ext}}(\boldsymbol{q}_{n+\frac{1}{2}})$ for $c = 1, \ldots, n_c$ or by slight modification of that (see Part II)
- if not possible: QR-decomposition of
  $(\boldsymbol{G}^c_{\text{ext}}(\boldsymbol{q}_n) \cdot \boldsymbol{P}_{\text{int}}(\boldsymbol{q}_n) \cdot \boldsymbol{P}^1_{\text{ext}}(\boldsymbol{q}_n) \cdot \cdots \cdot \boldsymbol{P}^{c-1}_{\text{ext}}(\boldsymbol{q}_n))^T$ yields implicitly $\mathbf{P}^c_{\text{ext}}(\boldsymbol{q}_n, \boldsymbol{q}_{n+1})$ for $c = 1, \ldots, n_c$ via formula (13)
- $\mathbf{P}(\boldsymbol{q}_n, \boldsymbol{q}_{n+1}) = \mathbf{P}_{\text{int}}(\boldsymbol{q}_n, \boldsymbol{q}_{n+1}) \cdot \mathbf{P}^1_{\text{ext}}(\boldsymbol{q}_n, \boldsymbol{q}_{n+1}) \cdot \cdots \cdot \mathbf{P}^{n_c}_{\text{ext}}(\boldsymbol{q}_n, \boldsymbol{q}_{n+1})$

(iv) solution of the resulting nonlinear algebraic system by applying one of the alternatives outlined in the sequel

alternative iv.1 (d'Alembert-type scheme)
solution of time-stepping scheme (11) for $\boldsymbol{q}_{n+1} \in \mathbb{R}^n$

alternative iv.2 (d'Alembert-type scheme with nodal reparametrization)
nodal reparametrization (14) $\boldsymbol{q}_{n+1} = \boldsymbol{F}_{\boldsymbol{q}_n}(\boldsymbol{\mu})$; solution of time-stepping scheme $(11)_{1,2}$ for $\boldsymbol{u} \in \mathbb{R}^{n-m}$

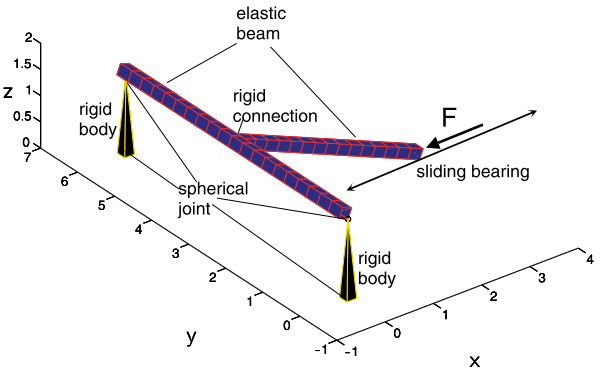

Fig. 4 Initial configuration of the spatial slider-crank mechanism

by a St. Venant–Kirchhoff-type stored energy function $W(\boldsymbol{\Gamma}, \boldsymbol{K})$ depending on the material strain measures $\boldsymbol{\Gamma}$, $\boldsymbol{K}$ (see [11, 30] and references therein for details), the constitutive equations

$$\boldsymbol{n} = \frac{\partial W}{\partial \boldsymbol{\Gamma}}, \qquad \boldsymbol{m} = \frac{\partial W}{\partial \boldsymbol{K}} \tag{69}$$

define the resulting axial and shear forces $\boldsymbol{n}$ and the resulting bending and torsional momenta $\boldsymbol{m}$ respectively. The end of the slider is supported by a sliding bearing which allows it to slide parallel to the x-axis in the xy-plane. The inertia properties of both elastic beams are characterized by the mass density per reference length $A_\rho = 20$ and the principal mass moments of inertia of the cross-section $M_\rho^1 = M_\rho^2 = 10$. The ends of the horizontal beam are connected via spherical joints to rigid bodies (see Example 5.1), which are modeled as pyramids of height $H = 1.5$ with square bases of edge length $A = 0.2$ and total mass $M = 1$ respectively. To allow true three-dimensional motion, both rigid bodies are supported by spherical joints fixed in space.

A force parallel to the x-axis $\boldsymbol{F}(t) = f(t)\boldsymbol{e}_1$ with

$$f(t) = \begin{cases} 1000 \sin(\pi t) & \text{for } t \leq 2, \\ 0 & \text{for } t > 2 \end{cases} \tag{70}$$

is applied at the end of the slider with a sinusoidal time variation for the first two seconds of motion. After the force is removed the system undergoes free vibration, since no other external loads are present. The results presented in the sequel have been obtained by solving the d'Alembert-type scheme (11) in conjunction with the nodal reparametrization (37). Figure 7 shows a series of snapshots of the motion and deformation of the slider-crank mechanism during the first and second revolution. The cuboids of the initially horizontal beam are coloured by a linear interpolation of the norm of the resulting momenta in the elements whereas the slider is coloured by the norm of the resultant forces. Thereby blue represents zero while red represents 3000. The deformations depicted in Fig. 7 are the original deformations, they have not been scaled for the illustration.

The orbit of the rigid connection point between the beams in Fig. 5 also emphasizes the large deformation the system is undergoing. It starts as a circle but soon leaves that path due to the large bending of the initially horizontal beam. The diagrams in Fig. 6 show the stress resultants in the rigidly connected elements for the horizontal beam on the left and for the slider on the right-hand side. One can see that the horizontal beam undergoes much bending deformation whereas in the slider the axial and shear forces dominate. Figure 8 shows that

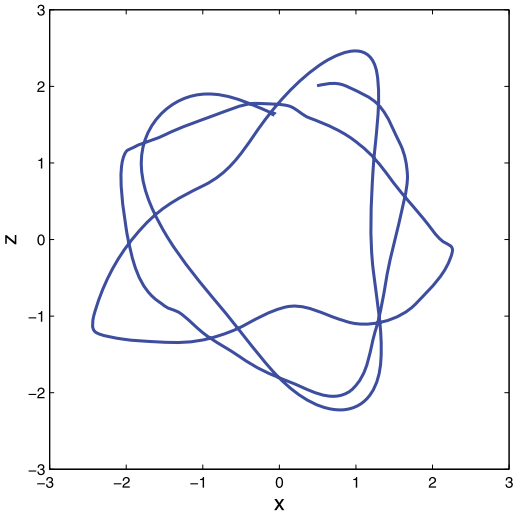

Fig. 5 Spatial slider-crank mechanism: orbit of the rigid connection point in the xz-plane

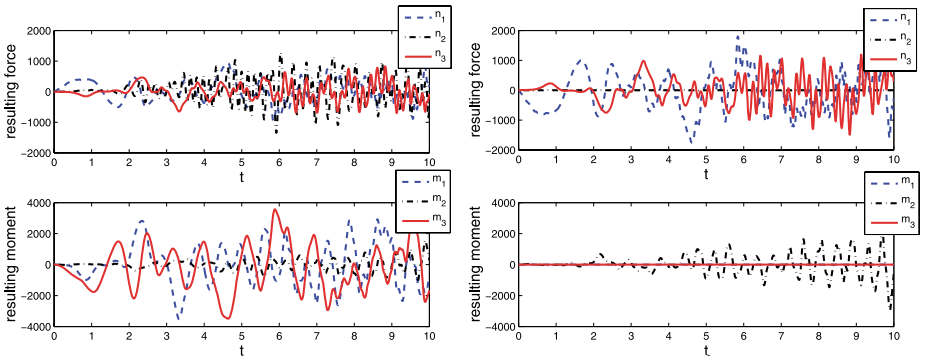

Fig. 6 Spatial slider-crank mechanism: stress resultants in rigidly connected elements in the initially horizontal beam (*left*) and in the slider (*right*) ($\Delta t = 0.01$)

after the removal of the external forces at $t = 2$ the total energy is conserved exactly. It also reveals that the strain energy amounts to a substantial part of the total energy.

5.2.1 Comparison

The same problem has been calculated using the constrained scheme (9). The schemes are equivalent, consequently the solutions are identical and both schemes fulfill the constraints exactly. Table 4 summarizes the simulations using both schemes. A remarkable difference is in the dimensions of the system of equations of motion. For both schemes, the first equation is solved for $\boldsymbol{v}_{n+1}$ and inserted into the second equation. Then, for the present problem, the constrained scheme requires the solution of 722 equations whereas the system for the d'Alembert-type scheme with nodal reparametrization is 214-dimensional. This has a big impact on the computational costs, the constrained scheme requires more than twice the CPU-time than the d'Alembert-type scheme with nodal reparametrization to simulate 10 seconds of motion and deformation of the slider-crank mechanism. For the time-step $\Delta t =$

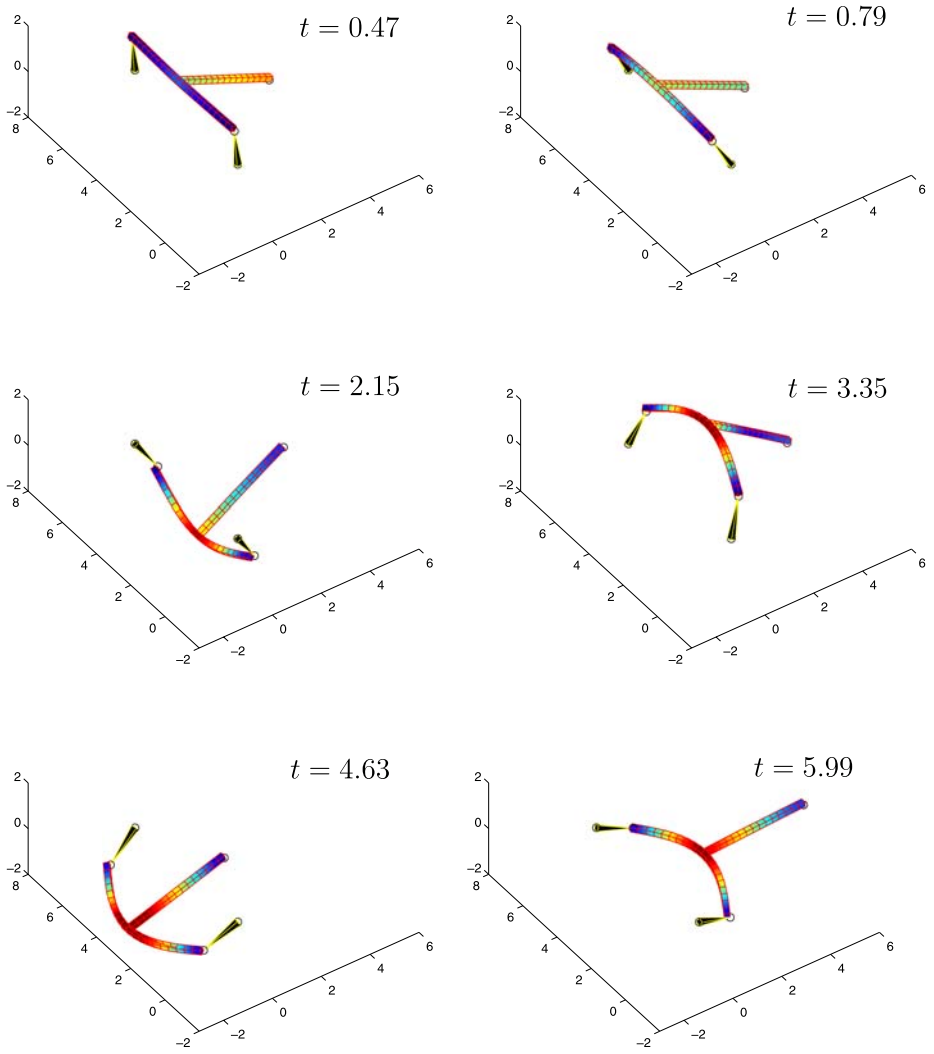

Fig. 7 Spatial slider-crank mechanism: snapshots of the motion and deformation at $t \in \{0.47, 0.79, 2.15, 3.35, 4.63, 5.99\}$

10^{-2} the condition number of the constrained scheme is of the order 10^{10} and it increases substantially for decreasing time-steps, whereas it is constant of the order 10^4 or less for arbitrary time-steps in the d'Alembert-type scheme.

5.3 Numerical example: intersecting shells

Next the flexible multibody system in Fig. 9, consisting of two rigid bodies and two elastic plates is considered. The data of each elastic plate is assumed to be as follows: length $L = 2$, width $b = 0.2$, thickness $h = 0.002$, Young's modulus $E = 7.3 \times 10^{10}$, Poisson's ratio $\nu = 0.25$ and mass density $\varrho = 2700$. Ten bi-linear shell elements are used for the discretization of each plate. The plates are rigidly connected to each other at one end. This leads

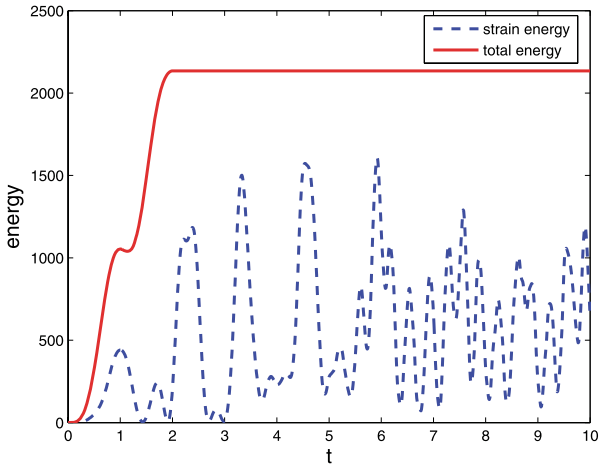

Fig. 8 Spatial slider-crank mechanism: energy ($\Delta t = 0.01$)

Table 4 Comparison of constrained scheme to d'Alembert-type scheme with nodal reparametrization for the example 'spatial slider-crank mechanism'

	Constrained scheme	d'Alembert-type scheme
Number of unknowns	722	214
$n = 468$, $m = 254$		
CPU-time	2.3	1
Condition number		
$\Delta t = 10^{-2}$	10^{10}	10^{4}
$\Delta t = 10^{-3}$	10^{11}	10^{3}
$\Delta t = 10^{-4}$	10^{14}	10^{3}

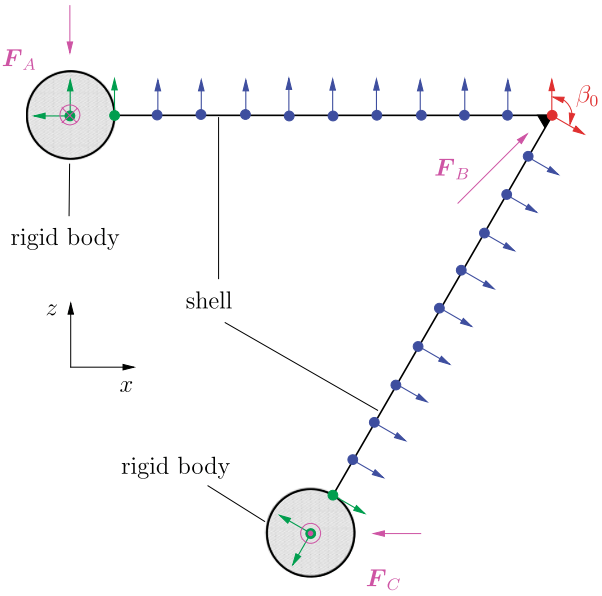

Fig. 9 Initial configuration of intersecting shells

to two nodal constraints of type 2 (see Table 1) with associated constraint functions (64), and angle $\beta_0 = 120°$. The other end of each plate is rigidly attached to a rigid body leading to further constraint equations. The inertia properties of both rigid bodies coincide with those of spheres with mass $M_\varphi = 10$ and radius $R = 0.2$.

External forces are acting on the system as indicated in Fig. 9, where

$$\boldsymbol{F}_A(t) = 2f(t)\begin{bmatrix} 0 \\ 2 \\ -2 \end{bmatrix}, \qquad \boldsymbol{F}_B(t) = 2f(t)\begin{bmatrix} 4 \\ 0 \\ 4 \end{bmatrix}, \qquad \boldsymbol{F}_C(t) = 2f(t)\begin{bmatrix} -2 \\ -2 \\ 0 \end{bmatrix}. \tag{71}$$

Here the load function $f(t)$ assumes the form of a hat function given by

$$f(t) = \begin{cases} 2f_m t/T & \text{for } 0 \le t \le T/2, \\ 2f_m(1 - t/T) & \text{for } T/2 < t \le T, \\ 0 & \text{for } t > T. \end{cases} \tag{72}$$

After the load period characterized by $f_m = 2$ and $T = 2$, the external loads vanish completely such that the algorithmic conservation properties can be checked. The tumbling mo-

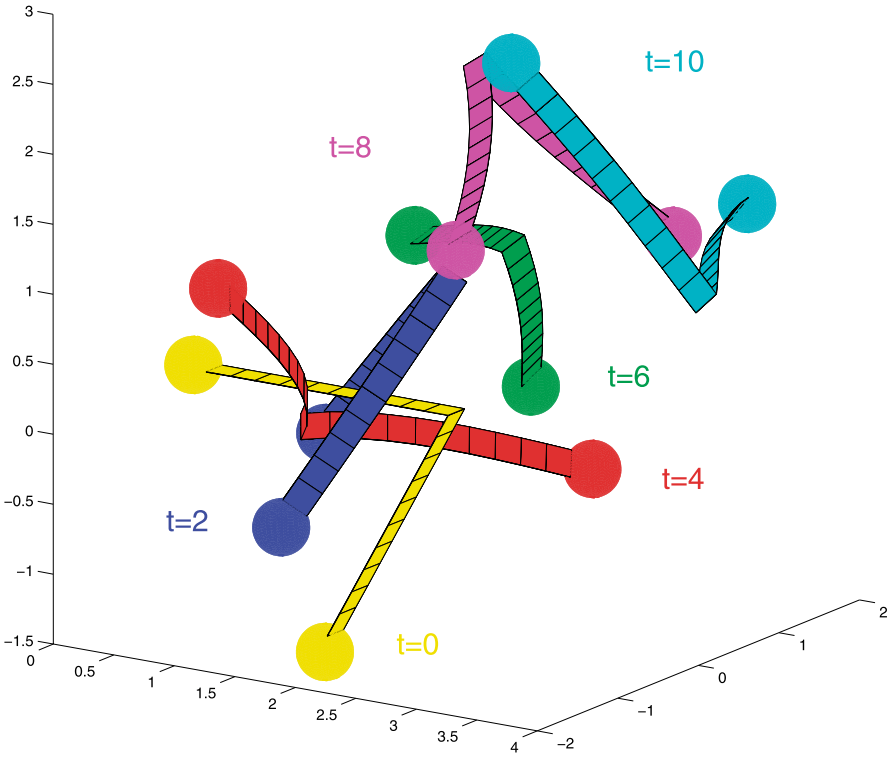

Fig. 10 Intersecting shells: snapshot of the motion and deformation at $t \in \{0, 2, 4, 6, 8, 10\}$

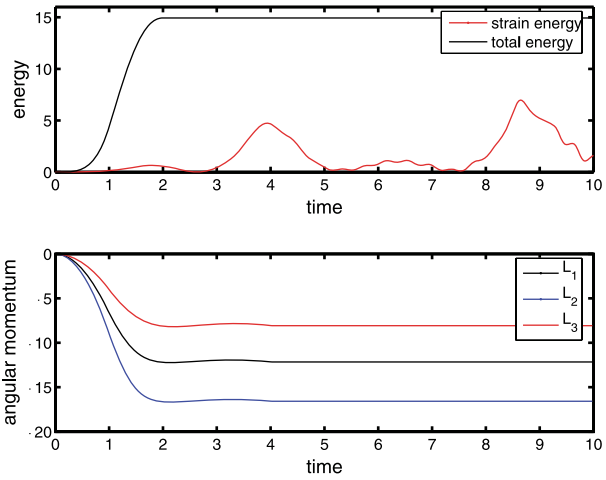

Fig. 11 Intersecting shells: strain energy, total energy and angular momentum $\boldsymbol{L} = L_i \boldsymbol{e}_i$ ($\Delta t = 0.02$)

tion of the system is illustrated by snapshots shown in Fig. 10. Throughout the whole calculation a constant time step $\Delta t = 0.02$ has been used. It can be observed from Fig. 11 that for $t > T$ the algorithm conserves the total energy as well as the vector of angular momentum. Furthermore, the constrained scheme consists of 288 equations, while the d'Alembert-type scheme with nodal reparametrization is 216-dimensional.

6 Conclusion

The discrete null space method performs a size-reduction of the temporal discrete system of equations of motion for mechanical systems subject to constraints. The constraint forces including the Lagrange multipliers are eliminated from the system, proceeding analogously to well-known size-reduction procedures from analytical mechanics. In this manner potential conditioning problems of the constrained scheme are removed.

The d'Alembert-type scheme provides exact constraint fulfillment at the time nodes and energy–momentum conservation along the solution. In particular because of the energy conservation, it is well suited for the simulation of elastic problems comprising high stiffnesses in the context of nonlinear elasticity. It can simulate systems of many degrees of freedom subject to a large number of constraints since it reduces the dimension of the system of equations to the minimal possible size. Holonomic as well as nonholonomic constraints (see [5]) can be treated likewise in a systematic way. For many applications, an explicit representation of the discrete null space matrix is feasible, e.g., for internal constraints in rigid bodies or structural elements, joints in multibody systems or bearings. Due to the independence of the condition number on the time-step, the method can cope with a wide range of time-steps.

References

1. Angeles, J., Lee, S.: The modeling of holonomic mechanical systems using a natural orthogonal complement. Trans. Can. Soc. Mech. Eng. **13**(4), 81–89 (1989)
2. Antmann, S.S.: Nonlinear Problems in Elasticity. Springer, Berlin (1995)
3. Bauchau, O.A., Choi, J.-Y.: On the modeling of shells in multibody dynamics. Multibody Dyn. Syst. 459–489 (2002)

4. Belytschko, T., Liu, W.K., Moran, B.: Nonlinear Finite Elements for Continua and Structures. Wiley, New York (2000)
5. Betsch, P.: A unified approach to the energy consistent numerical integration of nonholonomic mechanical systems and flexible multibody dynamics. GAMM Mitt. **27**(1), 66–87 (2004)
6. Betsch, P.: The discrete null space method for the energy consistent integration of constrained mechanical systems. Part I: Holonomic constraints. Comput. Methods Appl. Mech. Eng. **194**(50–52), 5159–5190 (2005)
7. Betsch, P., Leyendecker, S.: The discrete null space method for the energy consistent integration of constrained mechanical systems. Part II: Multibody dynamics. Int. J. Numer. Methods Eng. **67**(4), 499–552 (2006)
8. Betsch, P., Steinmann, P.: Constrained integration of rigid body dynamics. Comput. Methods Appl. Mech. Eng. **191**, 467–488 (2001)
9. Betsch, P., Steinmann, P.: Conserving properties of a time FE method. Part III: Mechanical systems with holonomic constraints. Int. J. Numer. Methods Eng. **53**, 2271–2304 (2002)
10. Betsch, P., Steinmann, P.: A DAE approach to flexible multibody dynamics. Multibody Syst. Dyn. **8**, 367–391 (2002)
11. Betsch, P., Steinmann, P.: Frame-indifferent beam finite elements based upon the geometrically exact beam theory. Int. J. Numer. Methods Eng. **54**, 1775–1788 (2002)
12. Bottasso, C.L., Borri, M., Trainelli, L.: Integration of elastic multibody systems by invariant conserving/dissipating algorithms. II. Numerical schemes and applications. Comput. Methods Appl. Mech. Eng. **190**, 3701–3733 (2001)
13. Brank, B., Korelc, J., Ibrahimbegović, A.: Dynamics and time-stepping schemes for elastic shells undergoing finite rotations. Comput. Struct. **81**, 1193–1210 (2003)
14. Büchter, N., Ramm, E.: Shell theory versus degeneration—a comparison in large rotation finite element analysis. Int. J. Numer. Methods Eng. **34**, 39–59 (1992)
15. Crisfield, M.A.: Non-linear Finite Element Analysis of Solids and Structures. Vol. I: Essentials. Wiley, New York (1991)
16. Crisfield, M.A., Jelenić, G.: Objectivity of strain measures in the geometrically exact three-dimensional beam theory and its finite-element implementation. Proc. Roy. Soc. Lond. A **455**, 1125–1147 (1999)
17. Géradin, M., Cardona, A.: Flexible Multibody Dynamics. Wiley, New York (2001)
18. Goicolea, J.M., Orden, J.C.: Dynamic analysis of rigid and deformable multibody systems with penalty methods and energy–momentum schemes. Comput. Methods Appl. Mech. Eng. **188**, 789–804 (2000)
19. Gonzalez, O.: Time integration and discrete Hamiltonian systems. J. Nonlinear Sci. **6**, 449–467 (1996)
20. Gonzalez, O.: Mechanical systems subject to holonomic constraints: differential-algebraic formulations and conservative integration. Phys. D **132**, 165–174 (1999)
21. Göttlicher, B.: Effiziente Finite-Element-Modellierung gekoppeler starrer und flexibler Strukturbereiche bei transienten Einwirkungen. PhD thesis, Universität Karlsruhe (2002)
22. Hughes, T.J.R.: The Finite Element Method. Linear Static and Dynamic Finite Element Analysis. Dover, New York (2000)
23. Hughes, T.J.R., Liu, W.K.: Nonlinear finite element analysis of shells. Part I: Three-dimensional shells. Comput. Methods Appl. Mech. Eng. **26**, 331–362 (1981)
24. Ibrahimbegović, A., Mamouri, S.: Finite rotations in dynamics of beams and implicit time-stepping schemes. Int. J. Numer. Methods Eng. **41**, 781–814 (1998)
25. Ibrahimbegović, A., Mamouri, S., Taylor, R.L., Chen, A.J.: Finite element method in dynamics of flexible multibody systems: modeling of holonomic constraints and energy conserving integration schemes. Multibody Syst. Dyn. **4**, 195–223 (2000)
26. Jelenić, G., Crisfield, M.A.: Interpolation of rotational variables in non-linear dynamics of 3d beams. Int. J. Numer. Methods. Eng. **43**, 1193–1222 (1998)
27. Jelenić, G., Crisfield, M.A.: Dynamic analysis of 3D beams with joints in presence of large rotations. Comput. Methods Appl. Mech. Eng. **190**, 4195–4230 (2001)
28. Kuhl, D., Ramm, E.: Generalized energy–momentum method for non-linear adaptive shell dynamics. Comput. Methods Appl. Mech. Eng. **178**, 343–366 (1999)
29. Leyendecker, S., Betsch, P., Steinmann, P.: Energy-conserving integration of constrained Hamiltonian systems—a comparison of approaches. Comput. Mech. **33**, 174–185 (2004)
30. Leyendecker, S., Betsch, P., Steinmann, P.: Objective energy–momentum conserving integration for the constrained dynamics of geometrically exact beams. Comput. Methods Appl. Mech. Eng. **195**, 2313–2333 (2006)
31. Marsden, J.E., Ratiu, T.S.: Introduction to Mechanics and Symmetry. A Basic Exposition of Classical Mechanical Systems. Texts in Applied Mathematics, vol. 17. Springer, Berlin (1994)
32. Munoz, J., Jelenić, G., Crisfield, M.A.: Master-slave approach for the modeling of joints with dependent degrees of freedom in flexible mechanisms. Commun. Numer. Methods Eng. **19**, 689–702 (2003)

33. Puso, M.A.: An energy and momentum conserving method for rigid-flexible body dynamics. Int. J. Numer. Methods Eng. **53**, 1393–1414 (2002)
34. Romero, I., Armero, F.: Numerical integration of the stiff dynamics of geometrically exact shells: an energy-dissipative momentum-conserving scheme. Int. J. Numer. Methods Eng. **54**, 1043–1086 (2002)
35. Romero, I., Armero, F.: An objective finite element approximation of the kinematics of geometrically exact rods and its use in the formulation of an energy–momentum scheme in dynamics. Int. J. Numer. Methods Eng. **54**, 1683–1716 (2002)
36. Sansour, J., Wagner, W., Wriggers, P.: An energy–momentum integration scheme and enhanced strain finite elements for the non-linear dynamics of shells. Nonlinear Mech. **37**, 951–966 (2002)
37. Simo, J.C.: On a stress resultant geometrically exact shell model. Part VII: Shell intersections with 5/6-DOF finite element formulations. Comput. Methods Appl. Mech. Eng. **108**, 319–339 (1993)
38. Simo, J.C., Rifai, M.S., Fox, D.D.: On a stress resultant geometrically exact shell model. Part VI: Conserving algorithms for non-linear dynamics. Int. J. Numer. Methods Eng. **34**, 117–164 (1992)
39. Simo, J.C., Tarnow, N.: A new energy and momentum conserving algorithm for the non-linear dynamics of shells. Int. J. Numer. Methods Eng. **37**, 2527–2549 (1994)
40. Taylor, R.L.: Finite element analysis of rigid-flexible systems. In: Ambrósio, J.A.C., Kleiber, M. (eds.) Computational Aspects of Nonlinear Structural Systems with Large Rigid Body Motion, vol. 179, pp. 62–84. IOS, Amsterdam (2001)
41. Warburton, G.B.: The Dynamical Behaviour of Structures. Pergamon, Elmsford (1976)